HYPK scaffolds the Nedd8 and LC3 proteins to initiate formation of autophagosome around polyneddylated huntingtin exon1 aggregates

Debasish Kumar Ghosh[1,*], and Akash Ranjan[1,*]

[1]Computational and Functional Genomics Group
Centre for DNA Fingerprinting and Diagnostics
Uppal, Hyderabad 500039, Telangana. India

*Corresponding authors

Email: akash@cdfd.org.in, dkghosh@cdfd.org.in
Telephone: +91-40-27216159
Fax: +91-40-27216006

ORCID:
Debasish Kumar Ghosh: 0000-0002-9196-0685
Akash Ranjan: 0000-0002-4582-1553

ABSTRACT

Selective degradation of protein aggregates by autophagy is an essential homeostatic process of safeguarding cells from the effects of proteotoxicity. Among the ubiquitin-like modifier proteins, Nedd8 conjugation to misfolded proteins is prominent in stress-induced protein aggregates, albeit the function of neddylation in autophagy is unclear. Here, we report that polyneddylation functions as a post-translational modification for autophagic degradation of proteotoxic-stress induced protein aggregates. We also show that HYPK functions as an autophagy receptor in the polyneddylation-dependent aggrephagy. The scaffolding function of HYPK is facilitated by its C-terminal ubiquitin-associated domain and N-terminal tyrosine-type LC3 interacting region which bind to Nedd8 and LC3 respectively. Both Nedd8 and HYPK are positive modulators of basal and induced-autophagy, leading to desensitizing cells from protein aggregates, such as aggregates of mutant huntingtin-exon1. Thus, we propose an additive role of neddylation and HYPK in clearance of protein aggregates by autophagy, resulting in cytoprotective effect during proteotoxic stress.

63 **INTRODUCTION**

64 Proteostasis is a dynamic process that ensures systemic maintenance of quality and quantity of
65 cellular proteome (1,2). Stress-induced proteins' misfolding and aggregation are countered by protein
66 quality control systems (PQCS) (3) which comprise a complex set of mechanisms, starting from guided
67 folding and oligomerization of nascent polypeptides by chaperones (4) to ordered elimination of
68 irreparable and non-functional proteins by proteasome and autolysosome machineries (5, 6). While the
69 soluble proteins and smaller protein complexes are cleaved by 26S proteasomal system, the phase-
70 separated insoluble protein aggregates are mainly degraded by autophagosomal/lysosomal pathway (7).
71 Macroautophagy (hereafter referred as autophagy) is a general mechanism that devours cellular
72 materials, such as damaged organelles, protein aggregates, intracellular pathogens etc., in a
73 membranous vesicle, referred as autophagosome, followed by hydrolytic degradation of
74 autophagosomal contents after fusion of autophagosome with lysosome (8). Initiation of
75 autophagosome formation from phagophore is critically regulated by several protein complexes (MTOR
76 complex, ULK1 complex, Vps34 complex, etc.) (9), whereas the maturation stage is more spontaneous
77 with the help of LC3, Beclin-1 and different ATG proteins (10).

78 Destabilization of cellular proteostasis by intrinsic or extrinsic stress causes formation of
79 heterogenous protein aggregates (11) which are selectively cleared by autophagy, often the process is
80 termed as aggrephagy (7). Ubiquitination of proteins is the activation signal for degradation of protein
81 aggregates by canonical autophagy pathway (12). The covalent linkage of ubiquitin to the target proteins
82 results from sequential activation and functioning of E1, E2 and E3 ligases (13). Lysine-63 (K63) type
83 polyubiquitin-linked protein aggregates are subjected to autophagic clearance (14). Although
84 ubiquitination is the major and global modulator of aggrephagy, ubiquitin-like modifiers (UBLs) are also
85 speculated to have contrasting functions in stress-induced autophagy. While the small ubiquitin-related
86 modifier 1 (SUMO1) suppresses autophagy (15), it is not known if other UBLs have regulatory functions
87 in autophagy. Particularly, understanding the function of Nedd8, which is a closely related protein to
88 ubiquitin, in proteostasis is not well characterized. Conjugation of Nedd8 to its substrate proteins,
89 mostly the cullin proteins (16), is mediated by its own set of ligase proteins (17). Interestingly,
90 neurodegenerative disease-related proteins (stress granule proteins, inclusion body proteins etc.) are
91 also neddylated (18, 19), indicating that neddylation of aggregation-prone proteins functions in
92 clearance of protein aggregates. During proteotoxic stress, neddylation also sequesters the vulnerable
93 nuclear proteins into aggregates (20). Moreover, thermal and redox stress also increase the cellular level
94 of polyneddylated proteins (21). While such neddylated proteins undergo NUB1-assisted turnover by
95 proteasomal system (22), the autophagy modulatory functions of Nedd8 remain unclear.

96 Autophagy receptor proteins are integral components in autophagosomal compartmentalization
97 of protein aggregates (23). Other than binding to ubiquitin or UBLs, autophagy receptors also recruit
98 LC3, leading to further assembly of autophagosomal machinery to phagophores. SQSTM1 (24), TAX1BP1
99 (25), TOLLIP (26) etc., are known ubiquitination-dependent autophagy receptors that promote
100 aggrephagy. However, the autophagy receptors of other UBLs are not well defined. In this context,
101 function of a member of intrinsically unstructured chaperone-like proteins (IUPs), named HYPK, in
102 autophagy modulation appears promising. HYPK functions in sequestering and reducing aggregates of

103 different cytosolic and nuclear proteins (27, 28). Previous studies from our group have showed that the
104 balance of structural convolution of HYPK is maintained by complex intra- and inter-molecular
105 interactions of its hydrophobic region, low complexity region and disordered nanostructure (29, 30).
106 Earlier studies found a putative acetyltransferase aiding function of HYPK at ribosome (31). In
107 *Caenorhabditis elegans*, HYPK forms proteasome blocking complexes (32), with a consequence in aging
108 of the organism (33).

109 In this article, we report the regulatory functions of UBLs, specifically Nedd8, and HYPK in
110 proteotoxic stress-induced aggrephagy. Assays for functional analysis reveal that polyneddylation of
111 proteins serves as a post-translational modification (PTM) mark for clearance of protein aggregates by
112 autophagy. In this pathway, HYPK functions as an autophagy receptor that scaffolds Nedd8 and LC3 by
113 using its ubiquitin-associated (UBA) domain and LC3 interacting region (LIR). Both neddylation of
114 proteins and HYPK act as aggrephagy inducer by helping autophagosome biogenesis around protein
115 aggregates, such as those arising from defective ribosomal products of puromycin-treated or
116 aggregation-prone huntingtin-exon1 expressing cells.

117 RESULTS

118 siRNA screen for ubiquitin-like proteins that modulate autophagic degradation of proteins during 119 proteotoxic stress

120 The existing and newly synthesized proteins are vulnerable to proteotoxic stress (34). Chemical
121 induction of intracellular proteotoxicity by puromycin occurs due to premature translation failure (35),
122 resulting in formation of defective ribosomal products (36) that are primarily cleared from cells by
123 autophagic degradation (37). While it is known that proteotoxic stress-induced protein aggregates are
124 ubiquitinated prior to their autophagic degradation, the role of other ubiquitin-like proteins (UBLs)
125 (**Supporting figure 1**) in this process is less understood. Hence, a screening of UBLs can shed more light
126 on their functions in autophagy. In order to conduct the screen of UBLs that drive the autophagic
127 degradation of proteins, we first determined the conditions of puromycin-induce proteotoxicity that
128 transduced its effects by increasing the autophagy flux without causing cell death. Autophagy flux was
129 monitored by a cell assay that measured the tandem fluorescence of RFP-GFP-LC3B (expressed in a
130 stable cell-line of MCF7) in different conditions. This is a standard autophagy flux assay in which RFP-
131 GFP-LC3B shows green (due to GFP) and red (due to RFP) double fluorescence in autophagosomes (AVs)
132 and only red fluorescence in autolysosomes (ALs), indicating spatiotemporal progress of formation and
133 maturation of AVs. Treatment of 15µg/ml puromycin (this concentration of puromycin was used in all
134 experiments unless otherwise stated) to cells significantly increased the number of GFP+/RFP+ LC3B
135 (AVs) and GFP-/RFP+ LC3B (ALs) puncta than untreated cells (**Figure 1A**). Conversion of native LC3B-I to
136 LC3B-II also increased during puromycin treatment (**Figure 1B**), indicating high autophagy flux. Thus, we
137 chose puromycin as a reproducible inducer of proteotoxic stress and autophagy in cells.
138 We screened siRNA combinations (6-18 siRNA/gene, 10nM) against six UBLs, including the
139 ubiquitin-siRNA (positive control), and a negative control-siRNA to understand the potency of the UBLs
140 in modulating autophagy during proteotoxic stress (timeline of screening experiment is in **Figure 1C**).
141 Other than the ubiquitin-siRNA, two siRNAs targeting the Nedd8 and FAT10 showed repression of

142 autophagy flux. Nedd8-siRNA and FAT10-siRNA prevented the formation of GFP+/RFP+ AVs and GFP-
143 /RFP+ ALs compared to control-siRNA during proteotoxic stress (**Figure 1C, 1D**). These two siRNAs also
144 reduced the conversion of LC3B-I to LC3B-II in normal growth condition (**Figure 1E, 1F**). Contrary to
145 Nedd8 and FAT10, downregulation of SUMO1 by siRNA increased formation of AVs/ALs and conversion
146 of LC3B-I to LC3B-II. Thus, Nedd8 and FAT10 showed autophagy inducing properties like ubiquitin,
147 whereas SUMO1 had opposite effect during proteotoxic stress.

148 Ubiquitin, Nedd8 and FAT10 appeared to be activators of basal autophagy than other UBLs.
149 Higher expression of these three proteins significantly increased autophagy as quantified by the
150 formation LC3B puncta in cells (**Figure 1G, 1H**). The effect of Nedd8 in increasing the basal autophagy
151 was similar to ubiquitin but higher than FAT10.

152 Ubiquitin-dependent autophagy of proteins involves the receptor function of p62/SQSTM1 (38).
153 Downregulation of ubiquitin expression caused reduction of autophagy flux and concomitant
154 accumulation of p62 in cells (**Figure 1I, 1J**). While knockdown of FAT10 showed similar phenotype,
155 Nedd8 downregulation did not show such effect on p62 levels in cells (**Figure 1I, 1J**). Thus, Nedd8
156 apparently modulated autophagy of proteins in p62 independent manner, possibly with the involvement
157 of other scaffolding protein(s).

158 **Proteotoxicity-induced Nedd8 granules are cleared by autophagy**

159 The preliminary finding from the knockdown (KD) screen that Nedd8 is a positive modulator of
160 autophagy led us to examine the crosstalk between protein neddylation and their autophagic removal
161 during proteotoxic stress. We observed formation of Nedd8 granules in puromycin-treated cells, but not
162 in the untreated cells (**Figure 2A**). The Nedd8 granules were high molecular weight neddylated protein
163 aggregates (**Figure 2B**). This observation was in-line with a previous study that also showed similar
164 accumulation of neddylated protein granules during proteotoxic stress (20). Interestingly, we found that
165 many of the puromycin-induced Nedd8 granules were also positive for LC3B (**Figure 2C, 2D**). Inhibition
166 of protein neddylation by a chemical inhibitor, MLN4924 (concentration: 1µM in culture medium of all
167 experiments unless otherwise stated), not only abolished the formation of Nedd8 granules in
168 puromycin-treated cells, but it also depleted the LC3B foci which were otherwise seen at the Nedd8
169 granules in puromycin-treated cells (**Figure 2C**). Accordingly, cotreatment of cells with puromycin and
170 MLN4924 decreased the basal level conversion of LC3B-I to LC3B-II compared to cells that were treated
171 only with puromycin (**Figure 2E**). These observations indicated that the neddylated protein granules
172 could be undergoing autophagic compartmentalization during proteotoxic stress.

173 Next, we examined if the neddylated granules were cleared through autophagy pathway by
174 knocking down one or more proteins of core autophagy machinery. Although puromycin initiated the
175 accumulation of Nedd8 granules, they were effectively cleared in control knockdown cells after the
176 washout of puromycin (**Figure 2F, 2G**). On the contrary, a significant number of Nedd8 granules
177 persisted in the ATG5 knockdown cells after puromycin washout (**Figure 2F, 2G**). Blocking the 26S
178 proteasomal pathway by knockdown of an essential proteasomal protein, PSMD8, also showed
179 accumulation of Nedd8 granules, even though almost five times lesser than the effect of ATG5
180 knockdown (**Figure 2F, 2G**). Taken together, these data suggest that proteotoxic stress causes formation
181 of neddylated substrate granules that are cleared by autophagy pathway.

182 To confirm the role of Nedd8 in autophagy, we further studied the expression of autophagy
183 markers during differential expression of Nedd8 protein. Higher expression of Nedd8 in MCF7 cells
184 caused increases lipidation of LC3B-I to LC3B-II, signifying the activation of autophagy pathway (**Figure**
185 **2H**). Knockdown of Nedd8 temporally reduced the cellular level of phosphoserine15-BECN1 (**Figure 2I**).
186 Such results provide the evidence that Nedd8 augments a noncanonical autophagy pathway to degrade
187 proteins.

188 **Polyneddylated aggregation-prone huntingtin exon1 is degraded by autophagy**

189 Having found that proteotoxicity-induced Nedd8 granules are cleared by autophagy, we were
190 interested to find if polyneddylated proteins are in general subjected to autophagic degradation.
191 Huntingtin is one of the few number of substrate proteins that undergo polyneddylation (39). Consistent
192 with the previous studies, we observed that the polyglutamine-expanded mutant huntingtin exon1
193 (htt97Qexon1) was polyneddylated (**Figure 3A**). Denaturing (with 1% SDS) immunoprecipitation of
194 Nedd8 (to purify only neddylated proteins and prevent purification of proteins that are noncovalently
195 associated with Nedd8) followed by immunoblotting against htt97Qexon1 showed the high molecular
196 weight neddylated htt97Qexon1 (**Figure 3A**). Neddylation of huntingtin exon1 aggregates in IMR-32 cells
197 was also evident from the observation of high Nedd8 colocalization/deposition with htt97Qexon1
198 aggregates (**Figure 3B**). Since a nonspecific protein (blue fluorescent protein, BFP) did not colocalize with
199 htt97Qexon1 (**Figure 3B**), it was apparent that neddylation of htt97Qexon1 was specific, and not just
200 trapping of Nedd8 with the sticky huntingtin exon1 aggregates.

201 In theory, huntingtin exon1 could be subjected to three different types of neddylation -
202 mononeddylation, polyneddylation and multi-mononeddylation. To understand the neddylation pattern
203 of htt97Qexon1, we generated a Nedd8 mutant construct in which all the lysine residues of Nedd8 were
204 mutated to arginine (Nedd8-allR) (**Supporting figure 2A**). This Nedd8-allR mutant cannot covalently
205 attach to another Nedd8 or Nedd8-allR molecule through lysine-linkage, thereby preventing the
206 formation of polyneddylated chains of Nedd8-allR. However, conjugation of Nedd8-allR to proteins can
207 form mononeddylated and multi-mononeddylated substrates. Coexpression of htt97Qexon1 with Nedd8
208 or Nedd8-allR showed that high molecular weight conjugated complexes of htt97Qexon1 formed only in
209 presence of Nedd8 (**Supporting figure 2B**). Nedd8-allR conjugation resulted in mononeddylated
210 htt97Qexon1, but not the polyneddylated or multi-mononeddylated htt97Qexon1.

211 During stress or higher expression of Nedd8, polyubiquitin chains also incorporate Nedd8 (40).
212 This phenomenon does not depend upon the Nedd8-activating enzyme (NAE1). Instead, Nedd8 is
213 activated by the ubiquitin-activating enzyme (UBA1) (41). In our experiments, the homogeneity of
214 polyneddylation of htt97Qexon1 was analyzed by using NAE1 and UBA1 inhibitors. Treatment of the
215 htt97Qexon1 expressing IMR-32 cells with NAE1 inhibitor, MLN4924, decreased polyneddylation of the
216 protein (**Supporting figure 2C**). Application of UBA1 inhibitor, MLN7243 (concentration: 1µM in culture
217 medium of all experiments unless otherwise stated), to the cells had no effects on the polyneddylation
218 of huntingtin exon1 (**Supporting figure 2C**).

219 To understand the effect of neddylation on huntingtin exon1 degradation by autophagy, we
220 measured the cellular level of htt97Qexon1 in varying expression conditions of Nedd8. Knockdown of
221 Nedd8 effectively decreased the degradation of htt97Qexon1 compared to control cells (**Figure 3C**).
222 Number of htt97Qexon1 aggregates also increased in the Nedd8-KD cells (**Figure 3D, 3E**). Exposure of
223 htt97Qexon1 expressing cells (in Nedd8-KD background) with proteasomal inhibitor (MG132;
224 concentration: 5µM in culture medium of all experiments unless otherwise stated) or autophagy
225 inhibitor (Bafilomycin-A1; concentration: 1µM in culture medium of all experiments unless otherwise
226 stated) showed further increase of htt97Qexon1 protein and its aggregates in terms of their numbers
227 and size (**Figure 3D, 3E, 3F**). In this respect, blocking the autophagy pathway had a more pronounced
228 effect than blocking the proteasomal pathway. Previous reports found that neddylated huntingtin could
229 be cleared through proteasomal pathway by the activity of NUB1 protein (39), possibly through the
230 activity of $p97^{UFD1/NPL4}$ Complex (42). However, given the condition that polyubiquitinated proteins, such
231 as huntingtin, could be redundantly degraded by both proteasomal and autophagosomal pathways (43),
232 we tested if polyneddylated htt97Qexon1 was also subjected to autophagosomal degradation. While
233 higher expression of Nedd8 enhanced the clearance of htt97Qexon1 from cells, downregulation of ATG5
234 prevented such Nedd8-facilitated clearance of htt97Qexon1 (**Figure 3G**). MG132 treatment to cells
235 ensured that neddylation-dependent degradation of htt97Qexon1 was not occurring through
236 proteasomal pathway. Since Nedd8 could assist the degradation of htt97Qexon1 in presence of MG132,
237 it was reasonable to understand that Nedd8 had regulatory functions in the autophagic degradation of
238 mutant huntingtin exon1. Overall, these observations showed that Nedd8 is an autophagy modulating
239 protein, and polyneddylation can serve as a signal of autophagic degradation of protein aggregates.

240 **HYPK is the receptor in neddylation-dependent autophagy**

241

242 The canonical degradation of polyubiquitinated proteins by autophagy requires the scaffolding
243 function of p62/SQSTM1 protein. p62 has a UBA and LC3 interacting region (LIR) which are used by the
244 protein to interact with ubiquitin and LC3 respectively. We expected that a protein with similar
245 scaffolding function would be required in the autophagy of polyneddylated proteins. The finding that
246 cellular level of p62 was unchanged during inhibition of neddylation-dependent autophagy (described in
247 first section of the results; **Figure 1I, 1J**), led us to turn our attention to identify the scaffolding protein
248 which is involved in the interaction with Nedd8 and LC3.

249 ***(I) HYPK interacts with Nedd8 through its C-terminal UBA domain***

250 Based on the fact that UBA domains recognize ubiquitin and UBLs (44), we tested a knockdown
251 screen for the effect of thirty UBA domain-containing proteins in retention of cellular Nedd8 granules.
252 Downregulation of five UBA domain-containing proteins significantly increased the number of
253 polyneddylated substrate granules in cells (**Figure 4A, 4B**); with HYPK knockdown showing highest
254 accumulation of neddylated granules (**Figure 4A**). To get further idea of an ideal binding of Nedd8 with
255 the UBA domains, we conducted computational docking/binding studies of Nedd8 with different UBA
256 domains of selected proteins. A higher free energy of assembly dissociation [ΔG(diss)] would indicate
257 stronger binding of Nedd8 with the respective UBA domain. The binding affinity of one of the UBA

258 domains of NUB1 with Nedd8 was highest, followed by the binding of HYPK-UBA with Nedd8 (**Figure 4C**),
259 implying that UBA domains of NUB1 and HYPK form thermodynamically stable complexes with Nedd8.

260 The functional binding of the UBA domain of NUB1 to Nedd8 (45) is known to be involved in
261 NUB1-facilitated degradation of neddylated proteins through proteasomal pathway. On the other hand,
262 aggregate-sequestering function of HYPK is linked to the degradation of the aggregation-prone proteins
263 in an unknown pathway (27). Thus, it is crucial to understand how HYPK delivers the protein aggregates
264 to degradation system.

265 HYPK structure shows the existence of a putative UBA domain in its C-terminal region (30). This
266 region is well conserved in the HYPK proteins of different organisms (**Supporting figure 3A**). A multiple
267 sequence alignment-based phylogenetic analysis to cluster the similar UBA domains of human proteins
268 directed to the observation that the sequence of the second UBA domain (UBA2) of NUB1 protein is
269 closest to the sequence of HYPK-UBA domain (**Supporting figure 3B**). Thus, we tested if HYPK is a Nedd8
270 interacting protein. HYPK could strongly bind to Nedd8 by using its UBA domain *in vitro* conditions.
271 Immunoprecipitation of Nedd8 from MCF7 cell lysate in non-denaturing condition, followed by
272 immunoblotting showed that both HYPK and HYPK-UBA could be pulled-down with Nedd8 (**Figure 4D**). A
273 reciprocal immunoprecipitation of HYPK, followed by immunoblotting for Nedd8 and HYPK was also
274 done to test which form of Nedd8 binds to HYPK. The immunoblot profile showed HYPK interaction with
275 both monomeric Nedd8 and polyneddylated chain (**Figure 4D**). Furthermore, we also observed that
276 HYPK and HYPK-UBA signals disappeared in the blots of denaturing (with 1% SDS) immunoprecipitation
277 of Nedd8 (**Supporting figure 3C**), indicating that HYPK and HYPK-UBA were not neddylated, but they
278 were noncovalently bound to Nedd8. HYPK and HYPK-UBA were also observed to show high spatial
279 colocalization with intracellular Nedd8 (**Figure 4E**).

280 We identified a set of critical residues in HYPK-UBA domain [aspartate-94 (D94), glutamate-101
281 (E101), leucine-113 (L113) and glycine-118 (G118); residue positions were numbered according to
282 human HYPK isoform-1; NCBI accession number: NP_057484.3] that were required for strong and
283 efficient binding of HYPK to Nedd8. These residues are typically conserved in the HYPK proteins of
284 different organisms (**Supporting figure 3A**). In order to understand the function of these amino acids in
285 HYPK binding to Nedd8, we generated different mutants of HYPK-UBA in which the conserved residues
286 were either mutated or deleted (**Figure 4F**). In the HYPK-UBA D94A, E101A construct, the D94 and E101
287 residues were mutated to alanine; whereas L113 and G118 residues were deleted in the HYPK-UBA
288 ΔL113, ΔG118 mutant. In the protein-protein interaction assays by surface plasmon resonance (SPR),
289 both the mutants displayed lower binding affinity for Nedd8 compared to the affinity of wild-type HYPK
290 and HYPK-UBA for Nedd8 (**Figure 4G**). It implied that the four conserved residues in HYPK-UBA were
291 necessary, but not sufficient, for HYPK-UBA interaction with Nedd8. Although the conserved amino acids
292 in HYPK-UBA were critical for HYPK binding to Nedd8, the neighboring residues possibly provided
293 additional support to the interaction. We also noted that the full-length HYPK protein had lower binding
294 affinity for Nedd8 than HYPK-UBA. The reduced binding affinity of HYPK for Nedd8 could be due to the
295 intramolecular interaction between the disorder nanostructure and low complexity region (LCR) of
296 HYPK, as shown in one of our previous studies (29). Such an intramolecular interaction can interfere in
297 the optimal binding of HYPK-UBA with Nedd8.

298 In the available crystal structure of HYPK (46), the E101 and G118 residues are exposed on the
299 surface of the protein, allowing these two residues to directly interact with the proximal residues of
300 Nedd8 in the HYPK-Nedd8 complex (**Figure 4H**). On the other hand, D94 and L113 residues are located
301 at the interface of two helices of the globular core of HYPK-UBA domain (**Figure 4H**). Thus, these
302 residues are more likely to be involved in stabilization of the HYPK-UBA domain rather than making
303 direct interactions with Nedd8.

304 ***(II) HYPK is an LC3 interacting protein***

305 To understand if HYPK is involved in facilitating the autophagic degradation of neddylated
306 proteins, we investigated the interaction of HYPK with LC3. HYPK lacks any conventional LIR which could
307 be represented by [W/Y/F]xx[L/V/I] sequence. However, an unbiased analysis of HYPK sequence
308 predicted a putative atypical LIR sequence represented by $Y_{49}AEE_{52}$ (**Figure 5A**). Such an atypical LIR with
309 an aromatic amino acid at first position and an acidic amino acid (instead of a hydrophobic amino acid)
310 at the fourth position is previously reported in the UBA5 protein (in the UBA5, the LIR is WGIE) (47). The
311 tyrosine-49 (Y49) is also conserved in the HYPK protein of various organisms (**Figure 5A**)

312 A non-denaturing immunoprecipitation assay with endogenous LC3B showed that HYPK was
313 coimmunoprecipitated with LC3B (**Figure 5B**). This observation was comparable with the findings of
314 another recent study that also reported proximity-dependent HYPK interaction with ATG8/LC3 in plants
315 (48). To validate if HYPK directly interacts with LC3 (LC3A and LC3B) and the GABARAP class of proteins
316 (GABARAP, GABARAPL1 and GABARAPL2), we conducted protein-protein interaction studies by pull-
317 down assays using recombinant proteins. We coexpressed 6xhistidine-tagged
318 LC3A/LC3B/GABARAP/GABARAPL1/GABARAPL2 and untagged HYPK in BL21DE3 strain of *Escherichia coli*
319 by using pETDuet-1 vector (pETDuet-1 vector allows coexpression of two recombinant proteins in T7
320 promoter expression system). Nickel-NTA beads affinity pull-down showed copurification of HYPK with
321 all the LC3 and GABARAP proteins (**Figure 5C**), suggesting that HYPK could globally interact with LC3 and
322 GABARAP subfamily proteins.

323 To probe the function of putative LIR of HYPK in LC3 binding, we used truncation mutations and
324 alanine scanning of HYPK as described in **Figure 5D**. The HYPK-UBA contained the C-terminal UBA
325 domain and HYPK-N84 construct was comprised of the N-terminal eighty-four amino acids (including the
326 putative LIR). The HYPK $Y^{49}AEE^{52}$> $A^{49}AAA^{52}$ was a site-directed mutagenesis construct in which all the
327 four residues in 49th-52nd amino acid region (YAEE) were mutated to alanine (AAAA) in the full-length
328 HYPK. The binding assays of recombinant proteins by SPR showed that HYPK and HYPK-N84, but not the
329 HYPK-UBA and HYPK $Y^{49}AEE^{52}$> $A^{49}AAA^{52}$, could bind to LC3B (**Figure 5E**), confirming that the LC3 binding
330 site of HYPK is located in the N-terminal region which contains the LIR at 49th-52nd amino acid stretch. To
331 validate the intracellular association of HYPK with LC3B, we traced the colocalization of HYPK, HYPK-N84,
332 HYPK-UBA and HYPK $Y^{49}AEE^{52}$> $A^{49}AAA^{52}$ with LC3B protein in MCF7 cells. Similar to the observations of
333 SPR study, only HYPK and HYPK-N84 showed high colocalization with LC3B (**Figure 4F**). These results
334 clearly show that HYPK interacts with LC3 by its atypical tyrosine-type (Y-type) LIR.

335 **HYPK modulates autophagy**

336 Having found that HYPK could interact with LC3 and Nedd8, we explored if HYPK modulated the
337 intracellular induction and flux of autophagy. Knockdown of HYPK reduced the basal level of cellular
338 autophagy, as seen by reduction of LC3B-II in HYPK-siRNA-treated cells compared to control cells (**Figure**
339 **6A**). HYPK knockdown also reduced the number of LC3B puncta, whereas HYPK overexpression
340 increased the number of LC3B puncta in MCF7 cells (**Figure 6B**), indicating that HYPK helps in formation
341 (i.e. induction) of autophagosomes. Imaging of HYPK overexpressing cells by transmission electron
342 microscopy also showed increased autophagosome formation (**Figure 6C**), while the control cells
343 contained significantly lesser number of autophagosomes (**Figure 6C**).

344 To further understand if HYPK was also involved in maintaining the autophagy flux, we
345 conducted a time-chase experiment to monitor the cellular levels of LC3B-II, BECN1 and ATG5-ATG12
346 during overexpression of HYPK. HYPK maintained the steady-state flux of autophagy by continuously
347 stimulating the lipidation of LC3B-I to LC3B-II without changing the cellular level of BECN1 and ATG5-
348 ATG12 (**Figure 6D**). Additionally, the maturation of autophagosomes to autolysosomes decreased in
349 HYPK knockdown cells. The count of RFP+/GFP- LC3B puncta (ALs) were almost four-fold less in HYPK
350 knockdown cells than control cells (**Figure 6E**). Thus, with these results, it was evident that HYPK had
351 enhancing function in selective autophagy induction and maturation.

352 **HYPK facilitates neddylation-dependent aggrephagy during proteotoxic stress**

353 To determine if HYPK clears the neddylated protein aggregates by autophagy during proteotoxic
354 stress, we analyzed the pattern of cellular distribution of HYPK in puromycin-treated cells. We observed
355 a time-dependent increase of HYPK foci, which colocalized with Nedd8 granules, in puromycin-treated
356 MCF7 cells (**Figure 7A, 7B**). It is, in fact, that we had previously shown the self-oligomerization of HYPK
357 upon heterogenous proteins aggregates (such as aggregates of α-Synuclein-A53T, SOD1-G93A,
358 htt97Qexon1 etc.) to sequester those protein aggregates (27). Complementary results in study showed
359 that the formation of HYPK foci is dependent upon neddylation-status of proteins in puromycin-treated
360 cells. HYPK could not form oligomeric granules in Nedd8-KD cells relative to control cells (**Figure 7C, 7D**).
361 Again, this result was consistent with the previously observed phenomenon that the metastable states
362 of UBA domain was required for self-association of HYPK (30).

363 To further investigate if HYPK has specific role in clearance of neddylated proteins through
364 autophagy, we checked the formation and clearance of puromycin-induced neddylated granules in
365 varying knockdown conditions of HYPK, autophagy machinery protein (ATG5) and proteasomal protein
366 (PSMD8). Neddylated protein granules accumulated and persisted even after the puromycin wash in
367 HYPK-KD and ATG5-KD cells (**Figure 7E, 7F**). After puromycin wash, the load of neddylated granules in
368 PSDM8-KD cells decreased to a minimum level that was comparable to control cells (**Figure 7E, 7F**).
369 Additionally, HYPK-KD decreased the conversion of LC3B-I to LC3B-II, which was otherwise observed in
370 Nedd8 overexpressing cells (**Figure 7G**). Such results implied that HYPK functions in the degradation of
371 neddylated proteins through selective autophagy.

372 Having established the global role of HYPK in neddylation-dependent autophagy, we finally
373 sought to elucidate if HYPK could channelize the degradation of neddylated htt97Qexon1 through

374 aggrephagy. In IMR-32 cells, HYPK colocalized with Nedd8-positive htt97Qexon1-GFP aggregates (**Figure**
375 **7H, 7I**). LC3B and Lamp1 also colocalized with the protein complexes of HYPK and htt97Qexon1GFP
376 (**Figure 7H, 7I**). It was also observed that HYPK facilitated the fusion of autophagosomal htt97Qexon1
377 aggregate with lysosomes to form autolysosomes (AL) (**Figure 6C**), suggesting that the complex of
378 HYPK/neddylated htt97Qexon1-GFP aggregates were not only subjected to be enclosed into autophagic
379 vacuoles, but they were also delivered to lysosomes for degradation. HYPK's role in autophagic
380 degradation of neddylated htt97Qexon1 was confirmed by following the degradation of the later
381 protein in different conditions that blocked the proteasomal or autophagy pathway by application of
382 specific inhibitors or knockdown of essential proteins of those pathways. HYPK-facilitated degradation of
383 htt97Qexon1 continued in presence of MG132 (**Figure 7J**). However, bafilomycin-A1 treatment of cells
384 had drastically prevented the capacity of HYPK to assist the degradation of htt97Qexon1 (**Figure 7J**). We
385 further validated HYPK's role as autophagy modulator of htt97Qexon1 in ATG5-KD/HYPK overexpressing
386 cells. Clearance of htt97Qexon1 was impeded in those cells than control cells (**Figure 7K**). Based on
387 these data, we conclude that autophagic degradation of neddylated proteins plays crucial roles in active
388 removal of toxic protein aggregates through the scaffolding functions of HYPK to Nedd8 and LC3 during
389 proteotoxic stress.

390 **DISCUSSION**

391 The various processes of clearance of intra- and extracellular protein aggregates are tailored to
392 maintain the cellular proteostasis in misfolded protein disorders and neurodegenerative
393 proteinopathies. The complexities in the mechanisms of autophagy are regulated by intriguing activity of
394 different regulatory proteins. In this study, we show that Nedd8 and HYPK are stress-responsive
395 regulators of degradation of protein aggregates by autophagy. The findings suggest that neddylation of
396 cytosolic protein aggregates, and their inclusion in autophagosomes by the receptor function of HYPK
397 (**Figure 8**) are parts of defensive response to control aggrephagy during proteotoxic stress.

398 In the physiological condition, neddylation has roles in stabilizing the cullin protein of cullin-ring
399 ligase (CRL) complexes (49), mitochondrial (50) protein etc., other than regulating the activity of
400 ubiquitin ligases (51) and maintaining proper localization of ribosomal proteins (52). In the stressed
401 conditions, polyneddylation of aggregation-prone proteins leads to their degradation by proteasomal
402 system. Here, we have shown that polyneddylation also prune the aggregated proteins for autophagic
403 degradation in such a way that complements the protein ubiquitination function. We conceive that
404 coexistence of polyubiquitination and polyneddylation pathways in aggrephagy is a part of fail-safe
405 mechanism with far reaching consequences. The differences of ubiquitination and neddylation codes, as
406 defined by the different kinds of lysine linkages in the chains, manifest alternative pathways of protein
407 degradation. While K63-linked polyubiquitin chain delivers proteins to autophagosome, this position-
408 specific lysine is absent in Nedd8. Thus, a unique, yet unknown, kind of neddylation linkage could
409 generate additional topological selectivity towards substrate proteins for autophagy. Additionally,
410 ubiquitination is a global process to most of the cellular proteins, and a large fraction of
411 polyubiquitinated proteins are intended for proteasomal degradation. Contrary to that, neddylation
412 could only be occurring to a limited number of proteins in the direction of aggrephagy. Thus,

413 redundancy of neddylation to such proteins in stressed conditions could compromise their
414 ubiquitination, thereby favouring the autophagic degradation.

415 Activation-dependent formation of homogeneous or mixed neddylation chains results in
416 differential fate of the substrate proteins. Formation of polyneddylation chain consisting of only Nedd8
417 protein depends upon the initial charging of the NAE1 (of the NAE1/UBA3 heterodimeric E1 ligase
418 complex) by activated Nedd8 (53). The observation that homogeneous polyneddylation of aggregation-
419 prone huntingtin exon1 directs it to autophagic degradation supports the notion that unmixed chains of
420 ubiquitin or Need8 are driving factors in protein degradation pathways, including autophagy. On the
421 other hand, stress-induced formation of mixed ubiquitin-Nedd8 chain results due to UBA1-dependent
422 incorporation of Nedd8 in polyubiquitin chain. Such ubiquitination system-induced Nedd8 addition to
423 ubiquitin chain has an effect in further aggregation of proteins, although that phenomenon still
424 participates in transient protection of cells from cytotoxicity (20, 54).

425 HYPK regulates aggrephagy through its interaction with LC3 and Nedd8, defining the pivotal
426 receptor function of this protein in a noncanonical autophagy pathway. The charged and hydrophobic
427 residues in the UBA domain of the C-terminus are necessary for HYPK binding to Nedd8. The UBA
428 domain is conserved in the longest isoform of HYPK protein of all species, signifying that Nedd8 binding
429 is an essential function of HYPK. Although it is unknown what type lysine-linkage in the polyneddylation
430 chain specifies the autophagosomal degradation of proteins, it is reasonable to speculate that the
431 unique sequence of HYPK-UBA domain is the determinant for recognizing such neddylation linkage.
432 While HYPK recognizes the polyneddylation chain on the protein aggregates, we cannot exclude that it
433 also binds to monomeric Nedd8 and neddylation chain of soluble proteins.

434 The LC3 binding function is attributed to the N-terminal LIR of HYPK. HYPK has an
435 unconventional LIR core sequence that lacks the hydrophobic amino acid at the fourth position.
436 Although the LIR of HYPK can be categorized as a 'composite LIR' (55), more structural studies can
437 expand the understanding if it can also function as 'half LIR' (56). Nevertheless, our preliminary studies
438 found that HYPK interacts with the LIR docking site (LDS) of LC3B, as LDS mutants of LC3B do not interact
439 with HYPK (data not shown). The absence of hydrophobic interactions at the fourth position of HYPK-LIR
440 could be compensated by an extended LIR that is inclusive of other hydrophobic interactions involving
441 not only the HP1 region but also the HP0 and HP2 regions of LC3 and GABARAP proteins. Consistent with
442 our previous report that the LIR-harboring N-terminal region of HYPK is a part of flexible and stretchable
443 disordered nanostructure (29), rearrangements of the essential interactions between HYPK-LIR and LDS
444 are possible. While such bonding rearrangements can lower the affinity of HYPK for LC3, oligomeric
445 HYPK binds multiple LC3 molecules, thereby increasing the overall binding strength. Moreover, the LIR is
446 present in the all the isoforms of HYPK, including the splice variant (isoform 2 - NP_001186814.1) that
447 lacks the UBA domain, suggesting that the LC3 binding and autophagy regulatory functions of HYPK are
448 conserved.

449 The ability of HYPK to regulate neddylation-dependent autophagy links this protein to the
450 general mechanisms of proteostasis. A workable model consists the proposition that proteotoxic stress
451 causes the formation of protein aggregates which are successively neddylated. HYPK interacts with the

452 Nedd8 of the neddylated protein aggregates, followed by sequestration of more HYPK with the
453 aggregates due to its cooperative self-association. Binding with Nedd8 also possibly results in HYPK's
454 transition from closed-to-open structure due to the loss of intramolecular interactions between the N-
455 terminal charged region and C-terminal low complexity region. The open conformer of HYPK recruits LC3
456 to the aggresomes, followed by assembly of downstream proteins of autophagy complex for initiation of
457 autophagosomal enclosure of protein aggregates.

458 Aggrephagy is a major mode of alleviating the load of the pathological protein aggregates in
459 cells of neurodegenerative disorders (NDs) (57). Our approach of a global screening of UBLs and UBA
460 domain-containing proteins has identified and validated the functions of Nedd8 and HYPK in modulation
461 of aggrephagy of huntingtin protein. Nedd8 and its conjugation machinery proteins have been identified
462 as modulators of NDs-associated proteins (58, 59). NUB1-assited recognistion of mutant huntingtin
463 protein serves as the activation signal for proteasomal degradation of huntingtin protein. Besides the
464 proteasomal pathway, our study showing that genetic and chemical perturbation of neddylation
465 pathway inhibits the aggrephagy of insoluble mutant huntingtin exon1 aggregates strongly suggests that
466 neddylation also causes recruitment of autophagosomal proteins to aggregates by generating Nedd8-
467 HYPK-LC3 complex. The constitutive neddylation of mutant huntingtin could be a segment of bipartite
468 surveillance system for simultaneous and dispensable degradation of the protein by different pathways.
469 The neddylation signal initially primes the soluble mutant huntingtin to proteasome, followed by
470 autophagosomal removal of insoluble aggregates of the protein. It is reported that NUB1 expression, but
471 not the NAE1 expression, is downregulated in knock-in mouse model of Huntington's disease (HD) (GEO:
472 GDS2912,) (60). Thus, it is interesting to test whether autophagy is the primary mode of degradation of
473 neddylated mutant huntingtin, although possibility of other supplementary mechanisms is also obvious.
474 This information can also be extrapolated to speculate that neddylation is prerequisite for autophagic
475 degradation of other labile proteins that are prone to misfolding and aggregation.

476 Similarly, the spatio-functional aspects of HYPK in proteostasis extend beyond its chaperone (61)
477 and aggregate-sequestering (27) functions to nonredundant role in huntingtin aggrephagy. Although
478 HYPK reportedly exerts its chaperone activity by interacting with the N-terminal region of huntingtin
479 (62), we reveal that aggrephagy is the mechanism of HYPK-mediated removal of huntingtin aggregates.
480 While the coupling of mutant huntingtin, HYPK, Nedd8 and LC3 can be dependent upon the context of
481 layers of huntingtin aggregates, it is also interesting to note that the expression of HYPK is regulated by
482 an array of factors like thermal stress (63), cellular aging (33) etc. Our previous studies showed that not
483 only huntingtin, but other disease-causing aggregation-prone proteins also elicit a HYPK coaggregation
484 response (27). Furthermore, the recruitment of HYPK to neddylated proteins can also be remotely
485 governed by the acetylation status of the target protein. The interaction of HYPK with the proteins of N-
486 acetyl transferase (NAT) complex (64) and acetylation-dependent neddylation of proteins (65) are
487 indicative of a complex crosstalk of post-translational modifications and HYPK recruitment in
488 multiprotein complexes during aggrephagy of misfolded proteins. Overall, the neddylation-dependent
489 aggrephagy takes place by synergistic effects of sequestration of HYPK with protein aggregates and
490 tethering function of HYPK.

Information of expression profile derived from gene expression omnibus (GEO) show that HYPK expression is not significantly changed in different NDs and brain diseases (**Supporting table 1**). Many of the HYPK interacting proteins also contain one or more aggregation-prone regions (data not shown), suggesting that proteostatic surveillance is general function of HYPK. Although HYPK is not a druggable target due to its noncatalytic function, modulation of its expression could be a potential mean to cope with the challenges of ND-associated protein aggregates.

In summary, this study identified the functionality of Nedd8 and HYPK as the modulators of autophagy in context of clearance of proteotoxic stress-induced and innate protein aggregates, thereby describing a novel and noncanonical mechanism of aggrephagy that can be utilized in HD therapeutics.

ACKNOWLEDGEMENTS

The authors extend their thankfulness to the Biocluster of National Centre for Biological Sciences (India) for providing the TEM facility. The authors also thank the members of CFG group for giving critical inputs in different experiments and manuscript writing. The personnel of sophisticated equipment facility of the research support service group of CDFD are acknowledged for the technical assistance in operating different instruments.

FUNDING

Research in CFG group is generously funded by the core grants of CDFD.

AUTHOR CONTRIBUTIONS

DKG: Conceptualization of the rationale of study, performed experiments, data analysis, manuscript writing. AR: Conceptualization of the rationale of study, data analysis, arrangement of funds, mentoring.

CONFLICT OF INTEREST

The authors report no competing conflict of interest.

545 ## MATERIALS and METHODS

546 ### Clones and plasmids

547 To clone the open reading frames (ORFs) of different genes, total RNA was isolated
548 (ThermoFischer Scientific [TFS], 12183018A) from IMR-32 cells, and cDNAs of corresponding mRNAs
549 were made by reverse transcription using the oligo-dT primer (Eurofins Genomics [EG]). ORFs of genes
550 were amplified from cDNAs by polymerase chain reaction (PCR) using specific primer sets (EG). The list
551 of clones and plasmids used in this study is given in **Table 1**. The general process of cloning was similar
552 to what was described in our previous studies (27, 66). Restriction digested PCR products and plasmids
553 were ligated, followed by the transformation of the ligated products in ultra-competent DH5α strain
554 of *Escherichia coli*. Positive clones were selected by colony PCR. All clones were sequenced at the
555 sophisticated equipment facility of the research support service group of CDFD.

556 **Table 1. Clones and plasmids**

Clone/Plasmid	Source	Identifier
FAT10-pcDNA3.1+	This work	
FLAG-HYPK-N84-pcDNA3.1+	This work	
FLAG-HYPK-UBA-pcDNA3.1+	This work	
FLAG- HYPK $Y_{49}AEE_{52}$>$A_{49}AAA_{52}$-pcDNA3.1+	This work	
GFP-Htt97Qexon1-pcDNA3.1+	27, 66	
Htt97Qexon1-pcDNA3.1+	This work	
HYPK-pcDNA3.1+	27	
Nedd8-pcDNA3.1+	This work	
6xHis Nedd8-pcDNA3.1+	This work	
6xHis Nedd8-allR-pcDNA3.1+	This work	
RFP-GFP-LC3B-pcDNA3.1+	This work	
S27A-pcDNA3.1+	This work	
SUMO1-pcDNA3.1	This work	
Ubiquitin-pcDNA3.1+	This work	
URM1-pcDNA3.1+	This work	
GABARAP-HYPK-pETDuet1	This work	
GABARAPL1-HYPK-pETDuet1	This work	
GABARAPL2-HYPK-pETDuet1	This work	
LC3A-HYPK-pETDuet1	This work	
LC3B-HYPK-pETDuet1	This work	
LC3B-pET21b	This work	
Nedd8-pET21b	This work	
HYPK-pET21b	29	
HYPK-N84-pET21b	This work	
HYPK-UBA-pET21b	29	
HYPK-UBA D94A, E101A-pET21b	This work	
HYPK-UBA ΔL113, ΔG118-pET21b	This work	
HYPK $Y_{49}AEE_{52}$>$A_{49}AAA_{52}$-pET21b	This work	
pcDNA3.1+	ThermoFischer Scientific	V790-20
pET21b	Novagen	69741-3

petDuet-1	Novagen	71146-3

557

558 **Site-directed mutagenesis**

559 Deletion mutants of HYPK were made by using specific primer sets (EG) in PCR-based method.
560 FLAG peptide sequence was introduced to different clones by incorporating the sequence in-frame at
561 the N-terminus of ORFs by using the forward primer (EG). Point mutations in HYPK (HYPK
562 $Y_{49}AEE_{52}$>$A_{49}AAA_{52}$), UBA domain of HYPK (UBA D94A, E101A; UBA ΔL113, ΔG118) and Nedd8 (allR – all
563 lysine-to-arginine) were created by using multiple primer sets (EG) in overlapping PCR method.
564 Mutations were confirmed by sequencing.

565 **Recombinant protein production and purification**

566 Recombinant HYPK, HYPK-UBA, HYPK-UBA D94A E101A, HYPK-UBA ΔL113 ΔG118, HYPK-N84,
567 HYPK $Y_{49}AEE_{52}$>$A_{49}AAA_{52}$, Nedd8, LC3A, LC3B, GABARAP, GABARAPL1, GABARAPL2 proteins were
568 produced by using a T7 expression system that was described by us in earlier studies (29, 67). The
569 bacterial expression clones (in pET21 and pETDuet-1 vectors) were separately transformed in the
570 BL21DE3 strain of *Escherichia coli*, followed by induction of protein synthesis by application of isopropyl
571 β-D-1-thiogalactopyranoside (IPTG, 1mM final concentration) (SA, I6758) in the culture medium (Luria
572 Bertani broth/ampicillin). After 12-18 hours of protein production at 18°C/180rpm, bacterial cells were
573 lysed by sonication in the lysis buffer [50mM Tris-Cl (pH: 8.0), 300mM NaCl, 10mM imidazole, 1mM
574 PMSF]. Cell lysate was cleared by centrifugation (14000g/40 minutes/4°C), followed by purification of
575 proteins by nickel ion-based affinity exchange column chromatography. The cleared lysate was run
576 through Ni^{+2}-NTA agarose beads (Qiagen [QA], 30250) to allow binding of the histidine-tagged
577 (recombinant) proteins to beads. The beads were subsequently washed with wash buffer [50mM Tris-Cl
578 (pH: 8.0), 300mM NaCl, 40mM imidazole], followed by elution of the proteins in elution buffer [50mM
579 Tris-Cl (pH: 8.0), 300mM NaCl, 300mM imidazole]. Proteins were dialyzed in different dialysis buffers
580 depending upon the requirements of downstream experiments. In all the experiments, >98% pure
581 proteins were used.

582 **Protein-protein binding assay by surface plasmon resonance**

583 The binding properties of HYPK, HYPK-UBA, HYPK-UBA D94A, E101A, HYPK-UBA ΔL113, ΔG118
584 with Nedd8; and HYPK, HYPK-N84, HYPK-UBA, HYPK $Y_{49}AEE_{52}$>$A_{49}AAA_{52}$ with LC3B were analyzed by
585 surface plasmon resonance (SPR) technique. Using the NHS/EDC reagent, 5nmole of Nedd8 or LC3B [in
586 acetate buffer (pH: 4.0)] was immobilized on a CM5 sensor chip (GE Healthcare Life Sciences, 29149604)
587 by amine coupling. The mobile phase analytes (HYPK, HYPK-UBA, HYPK-UBA D94A, E101A and HYPK-UBA
588 ΔL113, ΔG118, HYPK-N84, HYPK $Y_{49}AEE_{52}$>$A_{49}AAA_{52}$) were kept in HBS-EP buffer [10mM HEPES (pH: 7.5),
589 150mM NaCl, 3mM EDTA, 0.005% (v/v) Surfactant P20 (pH: 7.4)]. Analyte to ligand binding experiments
590 were done in the Biacore 3000 instrument (GE Healthcare Life Sciences) at 25°C. Analytes were injected
591 at a flowrate of 30µl/min, and the dissociation events were allowed for 10 minutes. Concentrations of
592 analytes were in the range of 40nM-25µM. Subtraction of nonspecific binding from the actual binding

593 response was done by measuring the mock binding on the immobilized surface of another channel.
594 Dissociation constants (K_d) were generated by assuming 1:1 Langmuir model of interaction.

595 **Cell culture and reagent treatment**

596 The MCF7 and IMR-32 cell-lines were procured from National Centre for Cell Sciences (NCCS,
597 India). MCF7 cells were cultured in advanced DMEM medium (TFS, 12491023) that was supplemented
598 with 10% fetal bovine serum (TFS, 26140095), 2mM L-glutamine (TFS, 25030164) and 1x antibiotic-
599 antimycotic solution (TFS, 11548876). IMR-32 cells were grown in neuronal culture medium (TFS, 88283)
600 supplemented with other components as mentioned for MCF7 cells. Cells were maintained in a humified
601 incubator at 37°C with 5% CO_2. Although cell lines were not authenticated, they were routinely checked
602 for mycoplasma contamination by using Venor™ GeM mycoplasma detection kit [Sigma-Aldrich (SA),
603 MP0025]. The stable expression of RFP-GFP-LC3B (in pcDNA3.1+) in MCF7 cell line, and GFP-
604 htt97Qexon1 (in pcDNA3.1+) or htt97Qexon1 (in pcDNA3.1+) in IMR-32 cell-line were selected by
605 keeping 2µM neomycin (SA, PHR1491) in the cell culture medium.

606 Puromycin (SA, P8833), MLN4924 [SA (Calbiochem), 505477), MG132 [SA (Calbiochem),
607 474790], Bafilomycin-A1 (SA, 196000), and MLN7243 (Aobious, AOB87172) were treated to cells with
608 specific concentration for defined time (as mentioned in different sections of results).

609 Clones and plasmids were transfected to subconfluent cells by using Lipofectamine 2000 (TFS,
610 11668019) and Opti-MEM (TFS, 31985070) medium following manufacturer's instructions. siRNAs were
611 transfected to cells by using Lipofectamine 3000 (TFS, L3000015). List of siRNAs are given in **Table 2**.
612 Transfected cells were harvested at different timepoints after transfection depending upon the
613 experimental requirements. In chase experiments, cells were intermittently harvested at an interval of 6
614 or 12 hours.

615 **Table 2. esiRNAs and siRNAs**

Target of esiRNA/siRNA	Source	Identifier
ATG5	Sigma-Aldrich	EHU085781
CBL	Sigma-Aldrich	EHU032851
CBL-B	Sigma-Aldrich	EHU074901
FAT10	Sigma-Aldrich	EHU230651
HYPK	Sigma-Aldrich	EHU096201
HUWE1	Sigma-Aldrich	EHU067731
MARK1	Sigma-Aldrich	EHU075901
MARK2	Sigma-Aldrich	EHU134171
MARK3	Sigma-Aldrich	EHU093021
MARK4	Sigma-Aldrich	EHU903821
Nedd8	Sigma-Aldrich	EHU112521
NUB1	Sigma-Aldrich	EHU020291
PSMD8	Sigma-Aldrich	EHU147871
Rad23A	Sigma-Aldrich	EHU027621
Rad23B	Sigma-Aldrich	EHU145881
RSC1A1	Sigma-Aldrich	EHU230881

S27A	Sigma-Aldrich	EHU112411
SIK1	Sigma-Aldrich	EHU138711
SQSTM1	Sigma-Aldrich	EHU027651
SUMO1	Sigma-Aldrich	EHU106621
TDRD3	Sigma-Aldrich	EHU037161
TNRC6C	Sigma-Aldrich	EHU080181
UBAC1	Sigma-Aldrich	EHU143751
UBAC2	Sigma-Aldrich	EHU141521
UBAP2	Sigma-Aldrich	EHU079831
UBE2K	Sigma-Aldrich	EHU091111
Ubiquitin	Santa Cruz Biotechnology	sc-29513
UBL7	Sigma-Aldrich	EHU060951
UBP5	Sigma-Aldrich	EHU025811
UBP13	Sigma-Aldrich	EHU003961
UBQL1	Sigma-Aldrich	EHU084751
UBQL2	Sigma-Aldrich	EHU029491
UBQL3	Sigma-Aldrich	EHU044731
UBQL4	Sigma-Aldrich	EHU109861
UBS3B	Sigma-Aldrich	EHU008351
UBXN1	Sigma-Aldrich	EHU157321
URM1	Sigma-Aldrich	EHU009021
VPS13D	Sigma-Aldrich	EHU123621
Universal negative control	Sigma-Aldrich	SIC001

Fractionation of soluble proteins and insoluble protein aggregates from cell lysate

To separate the insoluble polyneddylated protein aggregates and/or htt97Qexon1 aggregates from the soluble proteins, cells were scrapped from cell culture dishes in phosphate buffer saline (PBS, pH: 7.4), followed by lysis of cells in pre-chilled cell lysis buffer [LB - 50mM Tris-Cl (pH: 8.0), 50mM NaCl, 5mM $MgCl_2$, 0.2% Triton X-100, 0.5% Nonidet P-40, 1x protease inhibitor cocktail [SA, 11836170001)], phosphatase inhibitor (SA, PHOSS-RO)]. After keeping the cell suspension at 4°C for 15 minutes in LB, cell lysate was cleared by centrifugation at 14000g for 30 minutes (4°C). The supernatant contained the fraction of soluble proteins (SF). The precipitate, which contained insoluble fraction (IF) of protein aggregates and other cell debris, was resolubilized in LB that was supplemented with 1% SDS and 4M guanidinium chloride, followed by centrifugation of the suspension at 14000g for 30 minutes (4°C). The supernatant, which contained high-molecular weight polyneddylated proteins and/or htt97Qexon1 proteins, was finally dialyzed in dialysis buffer [DB – 50mM Tris-Cl (pH: 8.0), 50mM NaCl].

Immunoprecipitation and Immunoblotting

Immunoprecipitation (IP) of desired proteins were done from SF (2mg of protein) or SF (1mg of protein) + IF (1mg of protein) by using crosslink magnetic IP/co-IP method [TFS (Pierce Crosslink Magnetic IP/co-IP kit), 88805) following the manufacturer's protocol. Some IP experiments were done in denaturing conditions (with 1% SDS) as mentioned in the result section. List of antibodies used in IPs is given in **Table 3**.

635 In immunoblotting (IB), 60-80µg of total protein was added with 4x Laemmli buffer (Bio-Rad,
636 161-0747) and heated at 95°C for 10 minutes. Proteins were separated on 12% SDS-polyacrylamide gel,
637 followed by transfer of proteins from gel to polyvinylidene fluoride (PVDF) membrane (Amersham
638 Hybond P 0.45, GE Healthcare Life Sciences) and sequential use of primary and secondary antibodies
639 that are listed in **Table 3**. Intermittent washing was done by TBST buffer (pH: 7.4). Chemiluminescent
640 signal was generated by SuperSignal west femto maximum sensitivity substrate (TFS, 34094) and
641 detected by ChemiDoc XRS+ imaging system (Bio-Rad). Densitometric quantification of bands was done
642 in ImageJ2 software (68).

643 **Table 3. Antibodies**

Primary antibodies			
Target protein	**Species**	**Supplier**	**Catalogue number**
Alpha-tubulin	Mouse	Sigma-Aldrich	T9026
ATG5	Rabbit	Sigma-Aldrich	A0856
BECN1	Rabbit	Cell Signalling Technology	3738
Beta-tubulin	Mouse	Sigma-Aldrich	T8328
FAT10	Mouse	Abcam	ab168680
FLAG	Mouse	Sigma-Aldrich	F3165
His-tag	Mouse	Sigma-Aldrich	SAB2702218
HYPK	Rabbit	Sigma-Aldrich	SAB1101781
Lamp1	Mouse	Abcam	ab25630
LC3B	Rabbit	Abcam	ab48394
LC3B	Mouse	Cell Signalling Technology	83506
Nedd8	Rabbit	Abcam	ab194582
Nedd8	Mouse	ThermoFischer Scientific	MA5-17133
p62/SQSTM1	Mouse	Abcam	ab56416
polyQ (65Q)	Mouse	Sigma-Aldrich	P1874
pS15-BECN1	Rabbit	Cell Signalling Technology	84966S
S27A	Rabbit	Abcam	ab227011
SUMO1	Rabbit	Abcam	ab227424
Ubiquitin	Rabbit	Abcam	ab223613
URM1	Rabbit	Abcam	ab220490
Secondary antibodies (Immunoblotting)			
anti-rabbit IgG (whole molecule) peroxidase antibody	Goat	Sigma-Aldrich	A0545
anti-mouse IgG (whole molecule) peroxidase antibody	Rabbit	Sigma-Aldrich	A9044
Secondary antibodies (Immunocytochemistry)			
anti-Mouse IgG (H+L)-Alexa Fluor Plus 488	Goat	ThermoFischer Scientific	A32723
anti-Mouse IgG (H+L)-Alexa Fluor Plus 555	Goat	ThermoFischer Scientific	A32727

anti-Mouse IgG (H+L)-Alexa Fluor Plus 647	Goat	ThermoFischer Scientific	A32728
anti-Rabbit IgG (H+L)-Alexa Fluor Plus 488	Goat	ThermoFischer Scientific	A32731
Anti-Rabbit IgG (H+L)-Alexa Fluor Plus 555	Goat	ThermoFischer Scientific	A32732
anti-Rabbit IgG (H+L)-Alexa Fluor Plus 647	Goat	ThermoFischer Scientific	A32733

644

645 **Immunocytochemistry and fluorescence microscopy**

646 MCF7 or IMR-32 cells were grown on glass coverslips. The adherent cells were washed with PBS,
647 followed by fixation with methanol or 4% paraformaldehyde (in PBS). Cell permeabilization was done
648 with 0.2% TritonX-100 (in PBS, pH: 7.4), followed by blocking with 1% BSA (in PBS). Primary and
649 secondary antibodies (listed in **Table 3**) were sequentially given to cells with intermittent washing with
650 PBS. Cells were mounted in prolong antifade gold with or without DAPI (TFS, P36931; P10144). Images
651 were acquired in Zeiss LSM700 confocal laser scanning microscope (Carl Zeiss) with the 63x Plan-
652 Apochromat/ 1.4 NA oil/ DIC M27 objective. Images were processed in Zen-Lite 2010 software (Carl
653 Zeiss). Colocalization analysis of different proteins was done in Zen-Lite 2010 (blue edition) software
654 (Carl Zeiss) by using the colocalization algorithm. The Pearson's correlation coefficient was used as a
655 measure of colocalization of proteins.

656 The LC3B-positive autophagosome puncta, Nedd8 granules and htt97Qexon1-GFP aggregates in
657 cells were counted in Eclips Ti E (Nikon) microscope by using NIS-elements imaging software.

658 **Autophagy flux assay**

659 The GFP+/RFP+ and GFP-/RFP+ LC3B puncta represented the autophagosomes and
660 autolysosomes respectively, and their numbers were used to measure the autophagy flux as mentioned
661 in previous study (69). To monitor the autophagy flux in varying knockdown condition of different
662 proteins, cells were transfected with 10nM of esiRNA against target mRNA. The culture medium was
663 changed after 48 hours of transfection.

664 **Transmission electron microscopy**

665 IMR-32 cells were grown in culture dishes. HYPK or htt97Qexon1+HYPK were transfected to cells
666 by the procedure that is mentioned in cell culture section. Cells were detached from dishes by trypsin-
667 EDTA solution (SA, T3924). Detached cells were fixed in 1.5% (v/v) glutaraldehyde/4% (w/v)
668 formaldehyde (in 0.1M cacodylate buffer, pH: 7.4) solution for five hours, followed by washing of cells
669 with PBS (pH: 7.4) for few times. Dehydration of the cells was gradually done by sequentially keeping
670 them in 50%, 70% and 90% ethanol (15 minutes/solution). Cells were sectioned (1µm thick) in ultra-
671 microtome before placing them on 200 mesh copper grid (SA, G4776). Cell-section containing grids were
672 incubated in 0.05M glycine (in PBS) for 20 minutes. Grids were then washed with PBS, followed by
673 staining with aqueous uranyl acetate for 2 minutes. After the grids were washed with water, they were

674 transiently (for 15 seconds) exposed to lead citrate. Images were collected in Tecnai G2 Spirit Bio-TWIN
675 transmission electron microscope. Electron beam strength was 15kV and images were recorded in Gatan
676 Orins CCD camera.

677 **Computational studies**

678 ***Protein-protein docking*** – Structures of Nedd8 protein and the UBA domains of different human
679 proteins were curated (listed in **Table 4**) from the Protein Data Bank (70). Structures of the proteins
680 were optimized to add missing hydrogen atoms and assign bond orders in the protein preparation
681 wizard of Maestro 9.2 (Schrödinger) [forcefield: OPLS_2005, convergence of heavy atoms to root mean
682 square deviation (RMSD): 0.3 Å] as described in our previous studies (71, 72). Structures were
683 subsequently minimized in molecular modeling toolkit (73) by assisted model building with energy
684 refinement (AMBER) (74) simulation to 10^3 steepest descent iteration. Unrestrained protein-protein
685 docking of the finally prepared structures was done by using the PIPER program (75) in the BioLuminate
686 suite (Maestro 9.2, Schrödinger). The stability of complexes was measured by analyzing the ΔG(diss) in
687 the PDBePISA (Proteins, Interfaces, Structures and Assemblies) web server (76). Structures were
688 visualized and interpreted in PyMOL .

689 **Table 4. PDB identifiers of proteins' structures**

UBA domain of protein	PDB identifier	Reference
CBL	2OO9	77
CBL-B	2JNH	78
HUWE1	5LP8	79
HYPK	6C95	46
MARK1	2HAK	80
MARK2	1Y8G	81
MARK3	2QNJ	82
NBR1	2MGW	83
Nedd8	1NDD	84
NUB1	1WJU	Unpublished
Rad23A	1DV0	85
Rad23B	1P1A	86
SQSTM1	2K0B	87
TDRD3	1WJI	Unpublished
TNRC6C	2DKL	Unpublished
UBAC1	2DAI	Unpublished
UBAP1	1WGN	Unpublished
UBE2K	5DFL	88
Ubiquilin1	2JY6	89
Ubiquilin3	2DAH	Unpublished
Ubiquilin4	2KNZ	90
UBL7	2CWB	91
USP5	2DAG	Unpublished

690

691 ***Sequence alignment*** - The sequences of ubiquitin, UBLs and HYPK of different organisms were
692 obtained from protein database of National Center for Biotechnology Information (NCBI). Sequences of
693 UBA domains of different human proteins were curated from the SMART database (92). The alignments
694 of sequences were done in Clustal Omega (93).

695 ***Phylogenetic analysis*** - The sequence alignment file of the UBA domains of different human proteins
696 was saved in the phylip (.phy) format which was further used in the Phylip-3.695 software package. The
697 Seqboot, Protdist, Neighbor and Consense programs were sequentially run to analyze the phylogeny of
698 the UBA domains. The outfile of each program was taken as the input file of the next program. Details of
699 the parameters of each program are available upon request. The cladogram was generated in the
700 Treeview software.

701 **Statistical analysis**

702 The statistical significance of difference of means between groups were analyzed by two-tailed,
703 homoscedastic student's t-test. $P<0.05$ represented statistically significant difference.

704 **Graphics**

705 The graphics were made in Adobe Illustrator.

706 **DATA AVAILABILITY**

707 All the experimental protocols, data and resources of this study are available from the
708 corresponding authors on request.

709

710

711

712

713

714

715

716

717

718

719

720 **REFERENCES**

721 1. Labbadia, J. & Morimoto, R. I. The biology of proteostasis in aging and disease. *Annu Rev Biochem* **84**, 435-
722 464, doi:10.1146/annurev-biochem-060614-033955 (2015).
723 2. Klaips, C. L., Jayaraj, G. G. & Hartl, F. U. Pathways of cellular proteostasis in aging and disease. *J Cell Biol*
724 **217**, 51-63, doi:10.1083/jcb.201709072 (2018).
725 3. Chen, B., Retzlaff, M., Roos, T. & Frydman, J. Cellular strategies of protein quality control. *Cold Spring Harb*
726 *Perspect Biol* **3**, a004374, doi:10.1101/cshperspect.a004374 (2011).
727 4. Kim, Y. E., Hipp, M. S., Bracher, A., Hayer-Hartl, M. & Hartl, F. U. Molecular chaperone functions in protein
728 folding and proteostasis. *Annu Rev Biochem* **82**, 323-355, doi:10.1146/annurev-biochem-060208-092442
729 (2013).
730 5. Tanaka, K. The proteasome: overview of structure and functions. *Proc Jpn Acad Ser B Phys Biol Sci* **85**, 12-
731 36, doi:10.2183/pjab.85.12 (2009).
732 6. Glick, D., Barth, S. & Macleod, K. F. Autophagy: cellular and molecular mechanisms. *J Pathol* **221**, 3-12,
733 doi:10.1002/path.2697 (2010).
734 7. Lamark, T. & Johansen, T. Aggrephagy: selective disposal of protein aggregates by macroautophagy. *Int J*
735 *Cell Biol* **2012**, 736905, doi:10.1155/2012/736905 (2012).
736 8. Mizushima, N. Autophagy: process and function. *Genes Dev* **21**, 2861-2873, doi:10.1101/gad.1599207
737 (2007).
738 9. Hurley, J. H. & Young, L. N. Mechanisms of Autophagy Initiation. *Annu Rev Biochem* **86**, 225-244,
739 doi:10.1146/annurev-biochem-061516-044820 (2017).
740 10. Wesch, N., Kirkin, V. & Rogov, V. V. Atg8-Family Proteins-Structural Features and Molecular Interactions in
741 Autophagy and Beyond. *Cells* **9**, doi:10.3390/cells9092008 (2020).
742 11. Ruz, C., Alcantud, J. L., Vives Montero, F., Duran, R. & Bandres-Ciga, S. Proteotoxicity and
743 Neurodegenerative Diseases. *Int J Mol Sci* **21**, doi:10.3390/ijms21165646 (2020).
744 12. Chen, R. H., Chen, Y. H. & Huang, T. Y. Ubiquitin-mediated regulation of autophagy. *J Biomed Sci* **26**, 80,
745 doi:10.1186/s12929-019-0569-y (2019).
746 13. Zheng, N. & Shabek, N. Ubiquitin Ligases: Structure, Function, and Regulation. *Annu Rev Biochem* **86**, 129-
747 157, doi:10.1146/annurev-biochem-060815-014922 (2017).
748 14. Tan, J. M. *et al.* Lysine 63-linked ubiquitination promotes the formation and autophagic clearance of
749 protein inclusions associated with neurodegenerative diseases. *Hum Mol Genet* **17**, 431-439,
750 doi:10.1093/hmg/ddm320 (2008).
751 15. Lorente, M. *et al.* Inhibiting SUMO1-mediated SUMOylation induces autophagy-mediated cancer cell
752 death and reduces tumour cell invasion via RAC1. *J Cell Sci* **132**, doi:10.1242/jcs.234120 (2019).
753 16. Enchev, R. I., Schulman, B. A. & Peter, M. Protein neddylation: beyond cullin-RING ligases. *Nat Rev Mol*
754 *Cell Biol* **16**, 30-44, doi:10.1038/nrm3919 (2015).
755 17. Abidi, N. & Xirodimas, D. P. Regulation of cancer-related pathways by protein NEDDylation and strategies
756 for the use of NEDD8 inhibitors in the clinic. *Endocr Relat Cancer* **22**, T55-70, doi:10.1530/ERC-14-0315
757 (2015).
758 18. Jayabalan, A. K. *et al.* NEDDylation promotes stress granule assembly. *Nat Commun* **7**, 12125,
759 doi:10.1038/ncomms12125 (2016).
760 19. Mori, F. *et al.* Accumulation of NEDD8 in neuronal and glial inclusions of neurodegenerative disorders.
761 *Neuropathol Appl Neurobiol* **31**, 53-61, doi:10.1111/j.1365-2990.2004.00603.x (2005).
762 20. Maghames, C. M. *et al.* NEDDylation promotes nuclear protein aggregation and protects the Ubiquitin
763 Proteasome System upon proteotoxic stress. *Nat Commun* **9**, 4376, doi:10.1038/s41467-018-06365-0
764 (2018).
765 21. Lane, D. P. Stress, specificity and the NEDD8 proteome. *Cell Cycle* **11**, 1488-1489, doi:10.4161/cc.20073
766 (2012).

767 22. Li, J. *et al.* NEDD8 Ultimate Buster 1 Long (NUB1L) Protein Suppresses Atypical Neddylation and Promotes
768 the Proteasomal Degradation of Misfolded Proteins. *J Biol Chem* **290**, 23850-23862,
769 doi:10.1074/jbc.M115.664375 (2015).
770 23. Behrends, C. & Fulda, S. Receptor proteins in selective autophagy. *Int J Cell Biol* **2012**, 673290,
771 doi:10.1155/2012/673290 (2012).
772 24. Lippai, M. & Low, P. The role of the selective adaptor p62 and ubiquitin-like proteins in autophagy.
773 *Biomed Res Int* **2014**, 832704, doi:10.1155/2014/832704 (2014).
774 25. Sarraf, S. A. *et al.* Loss of TAX1BP1-Directed Autophagy Results in Protein Aggregate Accumulation in the
775 Brain. *Mol Cell* **80**, 779-795 e710, doi:10.1016/j.molcel.2020.10.041 (2020).
776 26. Lu, K., Psakhye, I. & Jentsch, S. Autophagic clearance of polyQ proteins mediated by ubiquitin-Atg8
777 adaptors of the conserved CUET protein family. *Cell* **158**, 549-563, doi:10.1016/j.cell.2014.05.048 (2014).
778 27. Ghosh, D. K., Roy, A. & Ranjan, A. Aggregation-prone Regions in HYPK Help It to Form Sequestration
779 Complex for Toxic Protein Aggregates. *J Mol Biol* **430**, 963-986, doi:10.1016/j.jmb.2018.02.007 (2018).
780 28. Ghosh, D. K. & Ranjan, A. An IRES-dependent translation of HYPK mRNA generates a truncated isoform of
781 the protein that lacks the nuclear localization and functional ability. *RNA Biol* **16**, 1604-1621,
782 doi:10.1080/15476286.2019.1650612 (2019).
783 29. Ghosh, D. K., Roy, A. & Ranjan, A. Disordered Nanostructure in Huntingtin Interacting Protein K Acts as a
784 Stabilizing Switch To Prevent Protein Aggregation. *Biochemistry* **57**, 2009-2023,
785 doi:10.1021/acs.biochem.7b00776 (2018).
786 30. Ghosh, D. K., Kumar, A. & Ranjan, A. Metastable states of HYPK-UBA domain's seeds drive the dynamics of
787 its own aggregation. *Biochim Biophys Acta Gen Subj* **1862**, 2846-2861, doi:10.1016/j.bbagen.2018.09.003
788 (2018).
789 31. Arnesen, T. *et al.* The chaperone-like protein HYPK acts together with NatA in cotranslational N-terminal
790 acetylation and prevention of Huntingtin aggregation. *Mol Cell Biol* **30**, 1898-1909,
791 doi:10.1128/MCB.01199-09 (2010).
792 32. Ayyadevara, S. *et al.* Proteins in aggregates functionally impact multiple neurodegenerative disease
793 models by forming proteasome-blocking complexes. *Aging Cell* **14**, 35-48, doi:10.1111/acel.12296 (2015).
794 33. Bell, R. *et al.* A human protein interaction network shows conservation of aging processes between
795 human and invertebrate species. *PLoS Genet* **5**, e1000414, doi:10.1371/journal.pgen.1000414 (2009).
796 34. Xu, G. *et al.* Vulnerability of newly synthesized proteins to proteostasis stress. *J Cell Sci* **129**, 1892-1901,
797 doi:10.1242/jcs.176479 (2016).
798 35. Azzam, M. E. & Algranati, I. D. Mechanism of puromycin action: fate of ribosomes after release of nascent
799 protein chains from polysomes. *Proc Natl Acad Sci U S A* **70**, 3866-3869, doi:10.1073/pnas.70.12.3866
800 (1973).
801 36. Yewdell, J. W., Anton, L. C. & Bennink, J. R. Defective ribosomal products (DRiPs): a major source of
802 antigenic peptides for MHC class I molecules? *J Immunol* **157**, 1823-1826 (1996).
803 37. Wenger, T. *et al.* Autophagy inhibition promotes defective neosynthesized proteins storage in ALIS, and
804 induces redirection toward proteasome processing and MHCI-restricted presentation. *Autophagy* **8**, 350-
805 363, doi:10.4161/auto.18806 (2012).
806 38. Ciuffa, R. *et al.* The selective autophagy receptor p62 forms a flexible filamentous helical scaffold. *Cell Rep*
807 **11**, 748-758, doi:10.1016/j.celrep.2015.03.062 (2015).
808 39. Lu, B. *et al.* Identification of NUB1 as a suppressor of mutant Huntington toxicity via enhanced protein
809 clearance. *Nat Neurosci* **16**, 562-570, doi:10.1038/nn.3367 (2013).
810 40. Schulman, B. A. & Harper, J. W. Ubiquitin-like protein activation by E1 enzymes: the apex for downstream
811 signalling pathways. *Nat Rev Mol Cell Biol* **10**, 319-331, doi:10.1038/nrm2673 (2009).
812 41. Leidecker, O., Matic, I., Mahata, B., Pion, E. & Xirodimas, D. P. The ubiquitin E1 enzyme Ube1 mediates
813 NEDD8 activation under diverse stress conditions. *Cell Cycle* **11**, 1142-1150, doi:10.4161/cc.11.6.19559
814 (2012).

42. Liu, S. *et al.* NEDD8 ultimate buster-1 long (NUB1L) protein promotes transfer of NEDD8 to proteasome for degradation through the P97UFD1/NPL4 complex. *J Biol Chem* **288**, 31339-31349, doi:10.1074/jbc.M113.484816 (2013).
43. Nedelsky, N. B., Todd, P. K. & Taylor, J. P. Autophagy and the ubiquitin-proteasome system: collaborators in neuroprotection. *Biochim Biophys Acta* **1782**, 691-699, doi:10.1016/j.bbadis.2008.10.002 (2008).
44. Su, V. & Lau, A. F. Ubiquitin-like and ubiquitin-associated domain proteins: significance in proteasomal degradation. *Cell Mol Life Sci* **66**, 2819-2833, doi:10.1007/s00018-009-0048-9 (2009).
45. Tanaka, T., Kawashima, H., Yeh, E. T. & Kamitani, T. Regulation of the NEDD8 conjugation system by a splicing variant, NUB1L. *J Biol Chem* **278**, 32905-32913, doi:10.1074/jbc.M212057200 (2003).
46. Gottlieb, L. & Marmorstein, R. Structure of Human NatA and Its Regulation by the Huntingtin Interacting Protein HYPK. *Structure* **26**, 925-935 e928, doi:10.1016/j.str.2018.04.003 (2018).
47. Habisov, S. *et al.* Structural and Functional Analysis of a Novel Interaction Motif within UFM1-activating Enzyme 5 (UBA5) Required for Binding to Ubiquitin-like Proteins and Ufmylation. *J Biol Chem* **291**, 9025-9041, doi:10.1074/jbc.M116.715474 (2016).
48. Macharia, M. W., Tan, W. Y. Z., Das, P. P., Naqvi, N. I. & Wong, S. M. Proximity-dependent biotinylation screening identifies NbHYPK as a novel interacting partner of ATG8 in plants. *BMC Plant Biol* **19**, 326, doi:10.1186/s12870-019-1930-8 (2019).
49. Keuss, M. J. *et al.* Unanchored tri-NEDD8 inhibits PARP-1 to protect from oxidative stress-induced cell death. *EMBO J* **38**, doi:10.15252/embj.2018100024 (2019).
50. Zhang, X. *et al.* Hepatic neddylation targets and stabilizes electron transfer flavoproteins to facilitate fatty acid beta-oxidation. *Proc Natl Acad Sci U S A* **117**, 2473-2483, doi:10.1073/pnas.1910765117 (2020).
51. Xie, P. *et al.* The covalent modifier Nedd8 is critical for the activation of Smurf1 ubiquitin ligase in tumorigenesis. *Nat Commun* **5**, 3733, doi:10.1038/ncomms4733 (2014).
52. Sundqvist, A., Liu, G., Mirsaliotis, A. & Xirodimas, D. P. Regulation of nucleolar signalling to p53 through NEDDylation of L11. *EMBO Rep* **10**, 1132-1139, doi:10.1038/embor.2009.178 (2009).
53. Gong, L. & Yeh, E. T. Identification of the activating and conjugating enzymes of the NEDD8 conjugation pathway. *J Biol Chem* **274**, 12036-12042, doi:10.1074/jbc.274.17.12036 (1999).
54. Lobato-Gil, S. *et al.* Proteome-wide identification of NEDD8 modification sites reveals distinct proteomes for canonical and atypical NEDDylation. *Cell Rep* **34**, 108635, doi:10.1016/j.celrep.2020.108635 (2021).
55. Johansen, T. & Lamark, T. Selective Autophagy: ATG8 Family Proteins, LIR Motifs and Cargo Receptors. *J Mol Biol* **432**, 80-103, doi:10.1016/j.jmb.2019.07.016 (2020).
56. Mandell, M. A., Kimura, T., Jain, A., Johansen, T. & Deretic, V. TRIM proteins regulate autophagy: TRIM5 is a selective autophagy receptor mediating HIV-1 restriction. *Autophagy* **10**, 2387-2388, doi:10.4161/15548627.2014.984278 (2014).
57. Yamamoto, A. & Simonsen, A. The elimination of accumulated and aggregated proteins: a role for aggrephagy in neurodegeneration. *Neurobiol Dis* **43**, 17-28, doi:10.1016/j.nbd.2010.08.015 (2011).
58. Richet, E. *et al.* NUB1 modulation of GSK3beta reduces tau aggregation. *Hum Mol Genet* **21**, 5254-5267, doi:10.1093/hmg/dds376 (2012).
59. Tanji, K. *et al.* Immunohistochemical localization of NUB1, a synphilin-1-binding protein, in neurodegenerative disorders. *Acta Neuropathol* **114**, 365-371, doi:10.1007/s00401-007-0238-1 (2007).
60. Hodges, A. *et al.* Brain gene expression correlates with changes in behavior in the R6/1 mouse model of Huntington's disease. *Genes Brain Behav* **7**, 288-299, doi:10.1111/j.1601-183X.2007.00350.x (2008).
61. Raychaudhuri, S., Sinha, M., Mukhopadhyay, D. & Bhattacharyya, N. P. HYPK, a Huntingtin interacting protein, reduces aggregates and apoptosis induced by N-terminal Huntingtin with 40 glutamines in Neuro2a cells and exhibits chaperone-like activity. *Hum Mol Genet* **17**, 240-255, doi:10.1093/hmg/ddm301 (2008).
62. Choudhury, K. R. & Bhattacharyya, N. P. Chaperone protein HYPK interacts with the first 17 amino acid region of Huntingtin and modulates mutant HTT-mediated aggregation and cytotoxicity. *Biochem Biophys Res Commun* **456**, 66-73, doi:10.1016/j.bbrc.2014.11.035 (2015).

63. Sakurai, H., Sawai, M., Ishikawa, Y., Ota, A. & Kawahara, E. Heat shock transcription factor HSF1 regulates the expression of the Huntingtin-interacting protein HYPK. *Biochim Biophys Acta* **1840**, 1181-1187, doi:10.1016/j.bbagen.2013.12.006 (2014).
64. Weyer, F. A. *et al.* Structural basis of HypK regulating N-terminal acetylation by the NatA complex. *Nat Commun* **8**, 15726, doi:10.1038/ncomms15726 (2017).
65. Scott, D. C. *et al.* Blocking an N-terminal acetylation-dependent protein interaction inhibits an E3 ligase. *Nat Chem Biol* **13**, 850-857, doi:10.1038/nchembio.2386 (2017)
66. Ghosh, D. K., Roy, A. & Ranjan, A. The ATPase VCP/p97 functions as a disaggregase against toxic Huntingtin-exon1 aggregates. *FEBS Lett* **592**, 2680-2692, doi:10.1002/1873-3468.13213 (2018).
67. Kumar, A., Ghosh, D. K., Ali, J. & Ranjan, A. Characterization of Lipid Binding Properties of Plasmodium falciparum Acyl-Coenzyme A Binding Proteins and Their Competitive Inhibition by Mefloquine. *ACS Chem Biol* **14**, 901-915, doi:10.1021/acschembio.9b00003 (2019).
68. Rueden, C. T. *et al.* ImageJ2: ImageJ for the next generation of scientific image data. *BMC Bioinformatics* **18**, 529, doi:10.1186/s12859-017-1934-z (2017).
69. Loos, B., du Toit, A. & Hofmeyr, J. H. Defining and measuring autophagosome flux-concept and reality. *Autophagy* **10**, 2087-2096, doi:10.4161/15548627.2014.973338 (2014).
70. Berman, H. M. *et al.* The Protein Data Bank. *Nucleic Acids Res* **28**, 235-242, doi:10.1093/nar/28.1.235 (2000).
71. Ghosh, D.K., Shrikondawar, A.N. & Ranjan A. Local structural unfolding at the edge-strands of beta sheets is the molecular basis for instability and aggregation of G85R and G93A mutants of Superoxide dismutase 1. *J Biomol Struct Dyn* **38**(3), 647-659, doi:10.1080/07391102.2019.1584125 (2019).
72. Ghosh, D.K., Kumar, A. & Ranjan A. T54R mutation destabilizes the dimer of Superoxide dismutase T54R by inducing steric clashes at the dimer interface. *RSC Advances* **10**, 10776-10788, DOI: 10.1039/C9RA09870D (2020).
73. Hinsen, K. The Molecular Modeling Toolkit: A New Approach to Molecular Simulations. *J. Comput. Chem.*, **21**(2), 79–85, doi:10.1002/(SICI)1096-987X(20000130) (2000).
74. Case, D. A. *et al.* The Amber biomolecular simulation programs. *J Comput Chem* **26**, 1668-1688, doi:10.1002/jcc.20290 (2005).
75. Kozakov, D., Brenke, R., Comeau, S. R. & Vajda, S. PIPER: an FFT-based protein docking program with pairwise potentials. *Proteins* **65**, 392-406, doi:10.1002/prot.21117 (2006).
76. Krissinel, E. & Henrick, K. Inference of macromolecular assemblies from crystalline state. *J Mol Biol* **372**, 774-797, doi:10.1016/j.jmb.2007.05.022 (2007).
77. Kozlov, G. *et al.* Structural basis for UBA-mediated dimerization of c-Cbl ubiquitin ligase. *J Biol Chem* **282**, 27547-27555, doi:10.1074/jbc.M703333200 (2007).
78. Zhou, Z. R. *et al.* Differential ubiquitin binding of the UBA domains from human c-Cbl and Cbl-b: NMR structural and biochemical insights. *Protein Sci* **17**, 1805-1814, doi:10.1110/ps.036384.108 (2008).
79. Sander, B., Xu, W., Eilers, M., Popov, N. & Lorenz, S. A conformational switch regulates the ubiquitin ligase HUWE1. *Elife* **6**, doi:10.7554/eLife.21036 (2017).
80. Marx, A. *et al.* Structural variations in the catalytic and ubiquitin-associated domains of microtubule-associated protein/microtubule affinity regulating kinase (MARK) 1 and MARK2. *J Biol Chem* **281**, 27586-27599, doi:10.1074/jbc.M604865200 (2006).
81. Panneerselvam, S., Marx, A., Mandelkow, E. M. & Mandelkow, E. Structure of the catalytic and ubiquitin-associated domains of the protein kinase MARK/Par-1. *Structure* **14**, 173-183, doi:10.1016/j.str.2005.09.022 (2006).
82. Murphy, J. M. *et al.* Conformational instability of the MARK3 UBA domain compromises ubiquitin recognition and promotes interaction with the adjacent kinase domain. *Proc Natl Acad Sci U S A* **104**, 14336-14341, doi:10.1073/pnas.0703012104 (2007).
83. Walinda, E. *et al.* Solution structure of the ubiquitin-associated (UBA) domain of human autophagy receptor NBR1 and its interaction with ubiquitin and polyubiquitin. *J Biol Chem* **289**, 13890-13902, doi:10.1074/jbc.M114.555441 (2014).

914 84. Whitby, F. G., Xia, G., Pickart, C. M. & Hill, C. P. Crystal structure of the human ubiquitin-like protein
915 NEDD8 and interactions with ubiquitin pathway enzymes. *J Biol Chem* **273**, 34983-34991,
916 doi:10.1074/jbc.273.52.34983 (1998).
917 85. Withers-Ward, E. S., Mueller, T. D., Chen, I. S. & Feigon, J. Biochemical and structural analysis of the
918 interaction between the UBA(2) domain of the DNA repair protein HHR23A and HIV-1 Vpr. *Biochemistry*
919 **39**, 14103-14112, doi:10.1021/bi0017071 (2000).
920 86. Ryu, K. S. *et al.* Binding surface mapping of intra- and interdomain interactions among hHR23B, ubiquitin,
921 and polyubiquitin binding site 2 of S5a. *J Biol Chem* **278**, 36621-36627, doi:10.1074/jbc.M304628200
922 (2003).
923 87. Evans, C. L., Long, J. E., Gallagher, T. R., Hirst, J. D. & Searle, M. S. Conformation and dynamics of the
924 three-helix bundle UBA domain of p62 from experiment and simulation. *Proteins* **71**, 227-240,
925 doi:10.1002/prot.21692 (2008).
926 88. Middleton, A. J. & Day, C. L. The molecular basis of lysine 48 ubiquitin chain synthesis by Ube2K. *Sci Rep* **5**,
927 16793, doi:10.1038/srep16793 (2015).
928 89. Zhang, D., Raasi, S. & Fushman, D. Affinity makes the difference: nonselective interaction of the UBA
929 domain of Ubiquilin-1 with monomeric ubiquitin and polyubiquitin chains. *J Mol Biol* **377**, 162-180,
930 doi:10.1016/j.jmb.2007.12.029 (2008).
931 90. Kieken, F., Spagnol, G., Su, V., Lau, A. F. & Sorgen, P. L. NMR structure note: UBA domain of CIP75. *J*
932 *Biomol NMR* **46**, 245-250, doi:10.1007/s10858-010-9397-9 (2010).
933 91. Chang, Y. G. *et al.* Solution structure of the ubiquitin-associated domain of human BMSC-UbP and its
934 complex with ubiquitin. *Protein Sci* **15**, 1248-1259, doi:10.1110/ps.051995006 (2006).
935 92. Ponting, C. P., Schultz, J., Milpetz, F. & Bork, P. SMART: identification and annotation of domains from
936 signalling and extracellular protein sequences. *Nucleic Acids Res* **27**, 229-232, doi:10.1093/nar/27.1.229
937 (1999).
938 93. Sievers, F. *et al.* Fast, scalable generation of high-quality protein multiple sequence alignments using
939 Clustal Omega. *Mol Syst Biol* **7**, 539, doi:10.1038/msb.2011.75 (2011).
940 94. Lesnick, T. G. *et al.* A genomic pathway approach to a complex disease: axon guidance and Parkinson
941 disease. *PLoS Genet* **3**, e98, doi:10.1371/journal.pgen.0030098 (2007).
942 95. Dunckley, T. *et al.* Gene expression correlates of neurofibrillary tangles in Alzheimer's disease. *Neurobiol*
943 *Aging* **27**, 1359-1371, doi:10.1016/j.neurobiolaging.2005.08.013 (2006).
944 96. Lee, J. M. *et al.* A novel approach to investigate tissue-specific trinucleotide repeat instability. *BMC Syst*
945 *Biol* **4**, 29, doi:10.1186/1752-0509-4-29 (2010).
946 97. Ferraiuolo, L. *et al.* Microarray analysis of the cellular pathways involved in the adaptation to and
947 progression of motor neuron injury in the SOD1 G93A mouse model of familial ALS. *J Neurosci* **27**, 9201-
948 9219, doi:10.1523/JNEUROSCI.1470-07.2007 (2007).
949 98. Chen-Plotkin, A. S. *et al.* Variations in the progranulin gene affect global gene expression in
950 frontotemporal lobar degeneration. *Hum Mol Genet* **17**, 1349-1362, doi:10.1093/hmg/ddn023 (2008).
951 99. Aydin, D. *et al.* Comparative transcriptome profiling of amyloid precursor protein family members in the
952 adult cortex. *BMC Genomics* **12**, 160, doi:10.1186/1471-2164-12-160 (2011).
953 100. Gatchel, J. R. *et al.* The insulin-like growth factor pathway is altered in spinocerebellar ataxia type 1 and
954 type 7. *Proc Natl Acad Sci U S A* **105**, 1291-1296, doi:10.1073/pnas.0711257105 (2008).
955 101. Han, M. H. *et al.* Janus-like opposing roles of CD47 in autoimmune brain inflammation in humans and
956 mice. *J Exp Med* **209**, 1325-1334, doi:10.1084/jem.20101974 (2012).
957 102. Lockstone, H. E. *et al.* Gene expression profiling in the adult Down syndrome brain. *Genomics* **90**, 647-660,
958 doi:10.1016/j.ygeno.2007.08.005 (2007).
959 103. Kim, M. Y. *et al.* hsp70 and a novel axis of type I interferon-dependent antiviral immunity in the measles
960 virus-infected brain. *J Virol* **87**, 998-1009, doi:10.1128/JVI.02710-12 (2013).
961 104. Gersten, M. *et al.* An integrated systems analysis implicates EGR1 downregulation in simian
962 immunodeficiency virus encephalitis-induced neural dysfunction. *J Neurosci* **29**, 12467-12476,
963 doi:10.1523/JNEUROSCI.3180-09.2009 (2009).
964 105. Hur, J. *et al.* The identification of gene expression profiles associated with progression of human diabetic
965 neuropathy. *Brain* **134**, 3222-3235, doi:10.1093/brain/awr228 (2011).

966 **FIGURES and LEGENDS**

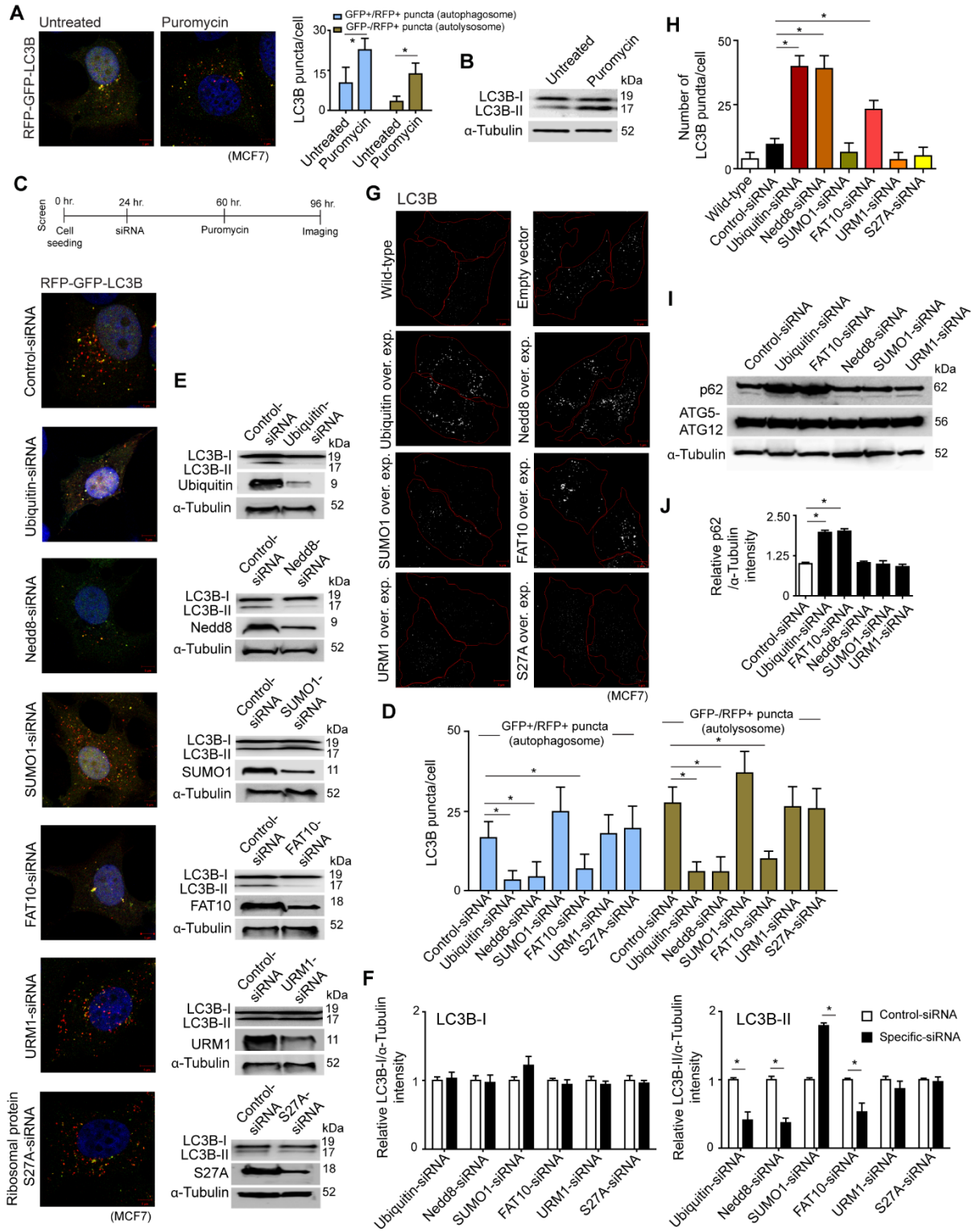

967

968 **Figure 1. siRNA screen for autophagy modulatory ubiquitin-like proteins in proteotoxic stress.** (A)
969 Stable RFP-GFP-LC3B expressing MCF7 cells were untreated or treated with puromycin [15µg/ml] for 24

970 hours. Left: confocal fluorescence microscopy images of GFP+/RFP+ LC3B autophagosomes and GFP-
971 /RFP+ LC3B autolysosomes. Right: Quantitative count [mean ± SD] of GFP+/RFP+ LC3B autophagosomes
972 and GFP-/RFP+ LC3B autolysosomes; ~ 100 cells analysed in each sample [* P<0.05]. (B) Representative
973 image of immunoblot of LC3B in lysate of untreated and puromycin-treated MCF7 cells. (C and D) Stable
974 RFP-GFP-LC3B expressing MCF7 cells transfected with different ubiquitin-like protein-specific siRNAs and
975 subsequent treatment of cells with puromycin for 36 hours. C: timeline of the screening experiment and
976 confocal fluorescence microscopy images of GFP+/RFP+ LC3B autophagosomes and GFP-/RFP+ LC3B
977 autolysosomes. D: mean ± SD number of GFP+/RFP+ LC3B autophagosomes and GFP-/RFP+ LC3B
978 autolysosomes; ~ 150 cells analysed in each experiment [* P<0.05]. (E and F) E: representative
979 immunoblot of LC3B from lysate of control-siRNA and UBL-specific siRNA-treated MCF7 cells. F:
980 densitometric quantification of LC3B-I and LC3B-II bands relative to α-tubulin of blots [* P<0.05]. (G and
981 H) MCF7 cells transfected with individual UBL-expressing clone. G: representative confocal
982 immunofluorescence images of LC3B puncta. H: average ± SD number of LC3B puncta/cell in different
983 UBL overexpression condition; ~ 150 cells analysed in each experiment [* P<0.05]. (I and J) Effect of
984 knockdown of UBLs on expression level of autophagy receptor p62 and autophagic proteins ATG5,
985 ATG12. I: representative immunoblots of p62 and ATG5-ATG12 in lysate of different UBL knockdown
986 cells. J: densitometric quantification of p62 bands relative to α-tubulin in immunoblots.

987 [α-tubulin is loading control in immunoblots. Scale bar in confocal microscopy images represents 5µm.
988 All the presented microscopy and immunoblot data are representative of at least three independent
989 experiments.]

990

991

992

993

994

995

996

997

998

999

1000

1001

1002

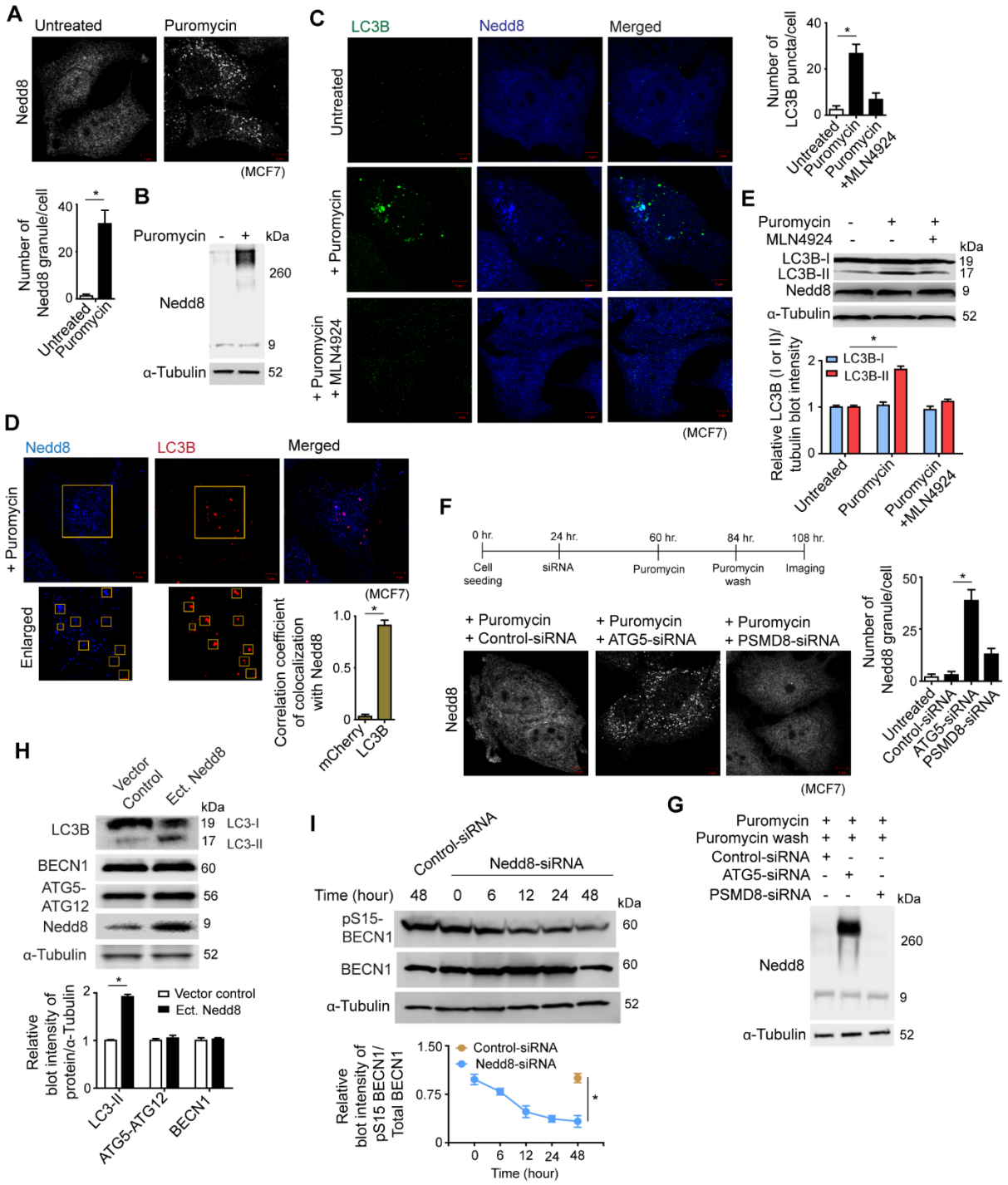

Figure 2. Nedd8 clears proteotoxic stress-induced protein aggregates by autophagy. (A and B) MCF7 cells untreated or treated with puromycin [15µg/ml] for 24 hours. A: confocal immunofluorescence microscopy images of Nedd8 granules, and mean ± SD quantification of Nedd8 granules; ~ 150 cells analysed in each sample [* P<0.05]. B: representative immunoblot of Nedd8 from cell extracts. (C) MCF7 cell were not treated or pretreated with 1µM MLN4924 for 12 hours and then exposed to puromycin [15µg/ml] for 24 hours. Confocal immunofluorescence microscopy images of Nedd8 and LC3B.

1010 Quantification of LC3B puncta with mean ± SD in cells; ~ 150 cells analysed in each sample [* P<0.05].
1011 (D) Representative confocal immunofluorescence microscopy image of colocalization of Nedd8 granules
1012 and LC3B in puromycin-treated [15µg/ml] MCF7 cells. Inset depicts enlarged images of Nedd8 and LC3B
1013 positive puncta marked with yellow rectangles. Correlation coefficient of colocalization of Nedd8
1014 granules with LC3B as compared to mCherry in MCF7 cells, ~ 50 cells analysed in each sample [* P<0.05].
1015 (E) Representative immunoblot of LC3B and Nedd8 in the condition described as in (c), with
1016 densitometric quantification of the LC3B-I and LC3B-II bands relative to α-tubulin in immunoblots [*
1017 P<0.05]. (F and G) ATG5, PSMD8 and control knockdown MCF7 cells were treated with puromycin
1018 [15µg/ml], followed by washout of puromycin with normal cell culture medium as presented in timeline
1019 of the experiment. F: confocal immunofluorescence microscopy images of Nedd8, and mean ± SD
1020 quantification of Nedd8 granules in different knockdown cells, ~ 150 cells analysed in each sample [*
1021 P<0.05]. G: Representative immunoblot of Nedd8 from the cell lysate of control, ATG5 and PSMD8
1022 knockdown MCF7 cells. (H) Representative immunoblot of autophagy marker proteins from lysate of
1023 control and Nedd8 overexpressing MCF7 cells. Densitometric quantification of bands of autophagy
1024 marker proteins relative to α-tubulin of blots [* P<0.05]. (I) Representative immunoblots of
1025 phosphoserine15-beclin-1 and beclin-1 [BECN1] in a time-chase experiment from lysate of control and
1026 Nedd8 knockdown MCF7 cells. Densitometric quantification of phosphoserine15-beclin-1 relative to
1027 beclin-1 in the immunoblots [* P<0.05].

1028 [α-tubulin is loading control in immunoblots. Scale bars in confocal microscopy images represent 5µm
1029 and 1µm for enlarged images. All the presented microscopy and immunoblot data are representative of
1030 at least three independent experiments.]

1031

1032

1033

1034

1035

1036

1037

1038

1039

1040

1041

1042

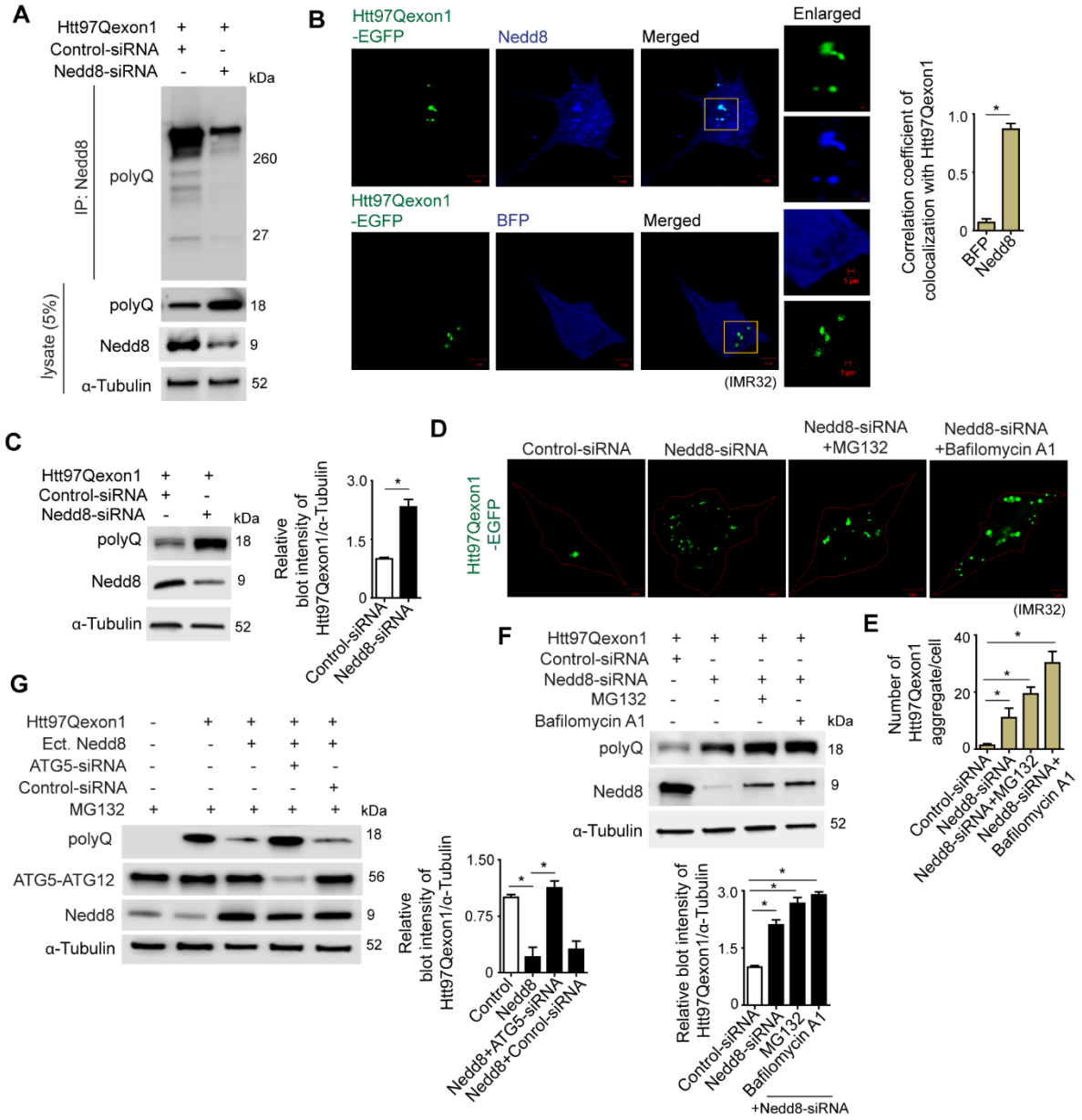

Figure 3. Neddylation mediates aggrephagy of mutant huntingtin exon1 protein aggregates. (A) Representative immunoblots of htt97Qexon [polyQ] and Nedd8 of denaturing immunoprecipitations of neddylated proteins from extract of stable htt97Qexon1 expressing IMR-32 cells transfected with control or Nedd8 siRNAs. (B) Confocal immunofluorescence image of colocalization of Nedd8 with htt97Qexon1-GFP in IMR-32 cells stably expressing htt97Qexon1-GFP. Quantification of colocalization coefficient of htt97Qexon1 GFP with Nedd8 compared to BFP, ~ 200 cells analysed in each sample [* P<0.05]. (C) Representative immunoblot of htt97Qexon1 and Need8 from lysate of htt97Qexon1-expressing IMR-32 cells transfected with control or Nedd8 siRNAs. Densitometric quantification of htt97Qexon1 bands relative to α-tubulin of blots [* P<0.05]. (D and E) Control or Nedd8 siRNA was transfected in stable htt97Qexon1-GFP expressing IMR-32 cells. Nedd8 knockdown cells were exposed to 5µM MG132 or 1µM bafilomycin-A1 for 24 hours. D: confocal fluorescence microscopy images of

1055 htt97exon1-GFP. E: quantification [mean ± SD] of htt97exon1-GFP aggregates, ~ 200 cells analysed in
1056 each sample [* P<0.05]. (F) Representative immunoblot of htt97Qexon1 and Nedd8 from experiments
1057 following the same procedure as that in (d), except that the IMR-32 cells stably expressed htt97Qexon1.
1058 Densitometric quantification of htt97Qexon1 bands relative to α-tubulin of blots [* P<0.05]. (G) Control
1059 or ATG5 siRNA was transfected in htt97Qexon1 and Nedd8 overexpressing IMR-32 cells in presence of
1060 5μM MG132. Representative immunoblots of htt97Qexon1 and Need8. Densitometric quantification of
1061 htt97Qexon1 bands relative to α-tubulin of blots [* P<0.05].

1062 [α-tubulin is loading control in immunoblots. Scale bars in confocal microscopy images represent 5μm.
1063 All the presented microscopy and immunoblot data are representative of at least three independent
1064 experiments.]

1065

1066

1067

1068

1069

1070

1071

1072

1073

1074

1075

1076

1077

1078

1079

1080

1081

1082

1083

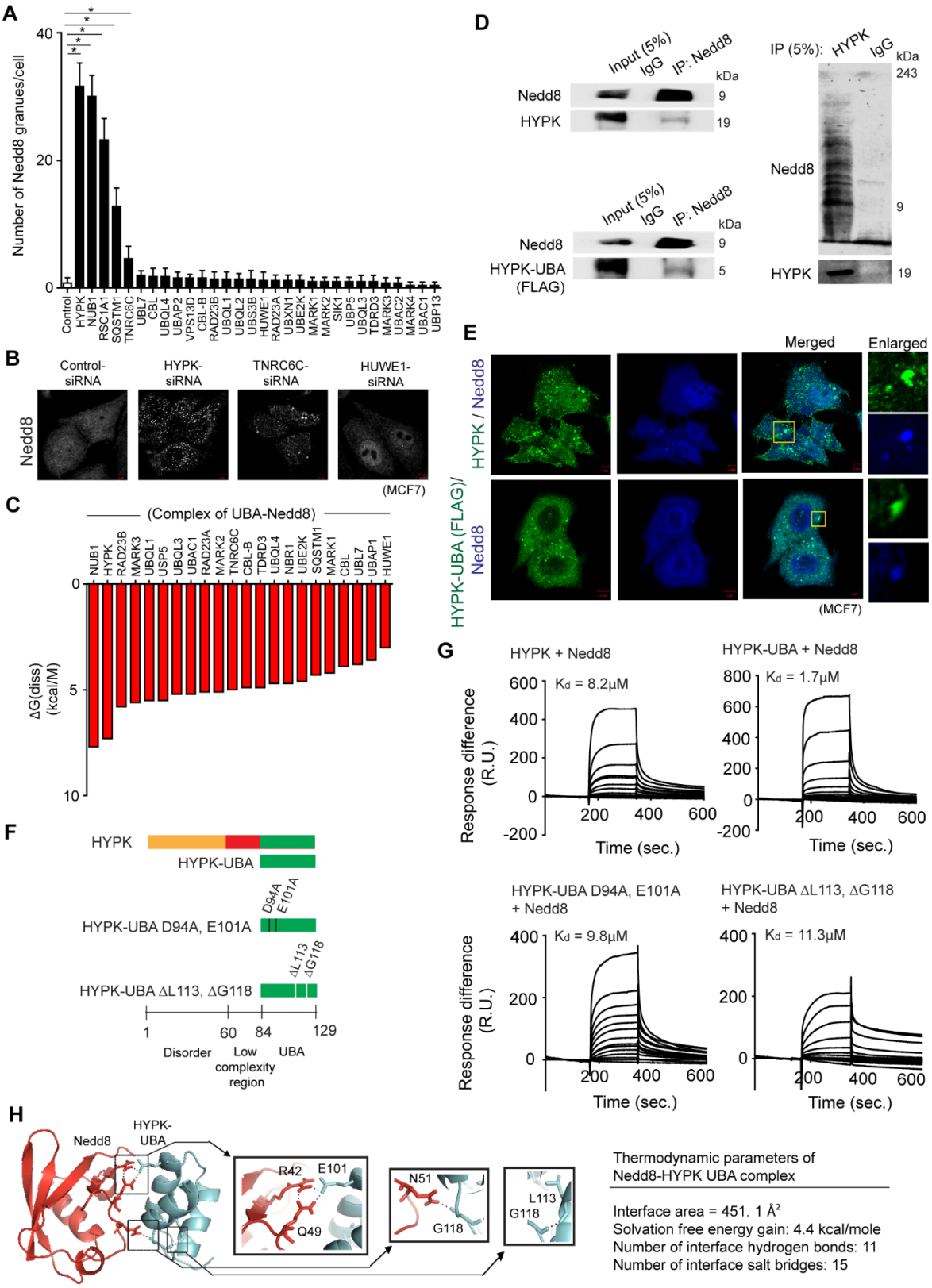

Figure 4. HYPK binds to Nedd8 by its UBA domain. (A and B) MCF7 cells were transfected with control or siRNA against different UBA domain containing proteins. A: number [mean ± SD] of Nedd8 granules in

1087 cells, ~ 300 cells analysed in each sample [* P<0.05]. B: Representative confocal immunofluorescence
1088 microscopy images of Nedd8. (C) *In silico* molecular docking of Nedd8 was done on UBA domains of
1089 selected human proteins. Free energy of dissociation of assemblies/complexes was computed in PISA
1090 webserver. (D) Representative immunoblots in non-denaturing conditions of – Left: Nedd8, HYPK and
1091 FLAG-tagged HYPK-UBA of immunoprecipitation of Nedd8 from cell lysate of MCF7 cells [FLAG-tagged
1092 HYPK-UBA was ectopically expressed]; Right: HYPK and Nedd8 of immunoprecipitation of HYPK from cell
1093 lysate of MCF7 cells. (E) Confocal immunofluorescence microscopy images of Nedd8, HYPK and FLAG-
1094 tagged HYPK-UBA in MCF7 cells. (F) Representation of HYPK, its UBA domain and different mutants of
1095 HYPK-UBA domain that were used in this section of study. HYPK-UBA domain contained the C-terminal
1096 45 amino acid region; the D94 and E101 residues were mutated to alanine in HYPK-UBA D94A, E101A
1097 construct; the L113 and G118 residues were deleted in HYPK-UBA ΔL113, ΔG118 construct. (G)
1098 Quantitative binding responses and affinities of interactions between recombinant HYPK/HYPK-UBA/
1099 HYPK-UBA D94A, E101A/HYPK-UBA ΔL113, ΔG118 and Nedd8 probed by surface plasmon resonance
1100 assays. Dissociation constants [K_d value] were calculated by using 1:1 Langmuir model of binding. (H)
1101 Structural basis and thermodynamic parameters of interactions between Nedd8 and HYPK-UBA in the
1102 HYPK-Nedd8 complex. Left: predicted structure of complex of HYPK and Nedd8. Right: the conserved
1103 residues in HYPK-UBA and their interaction partners in Nedd8 are shown with stick representation.
1104 Hydrogen bonds are highlighted with black dotted line.

1105 [α-tubulin is loading control in immunoblots. Scale bars in confocal microscopy images represent 5µm.
1106 All the presented microscopy and immunoblot data are representative of at least three independent
1107 experiments.]

1108

1109

1110

1111

1112

1113

1114

1115

1116

1117

1118

1119

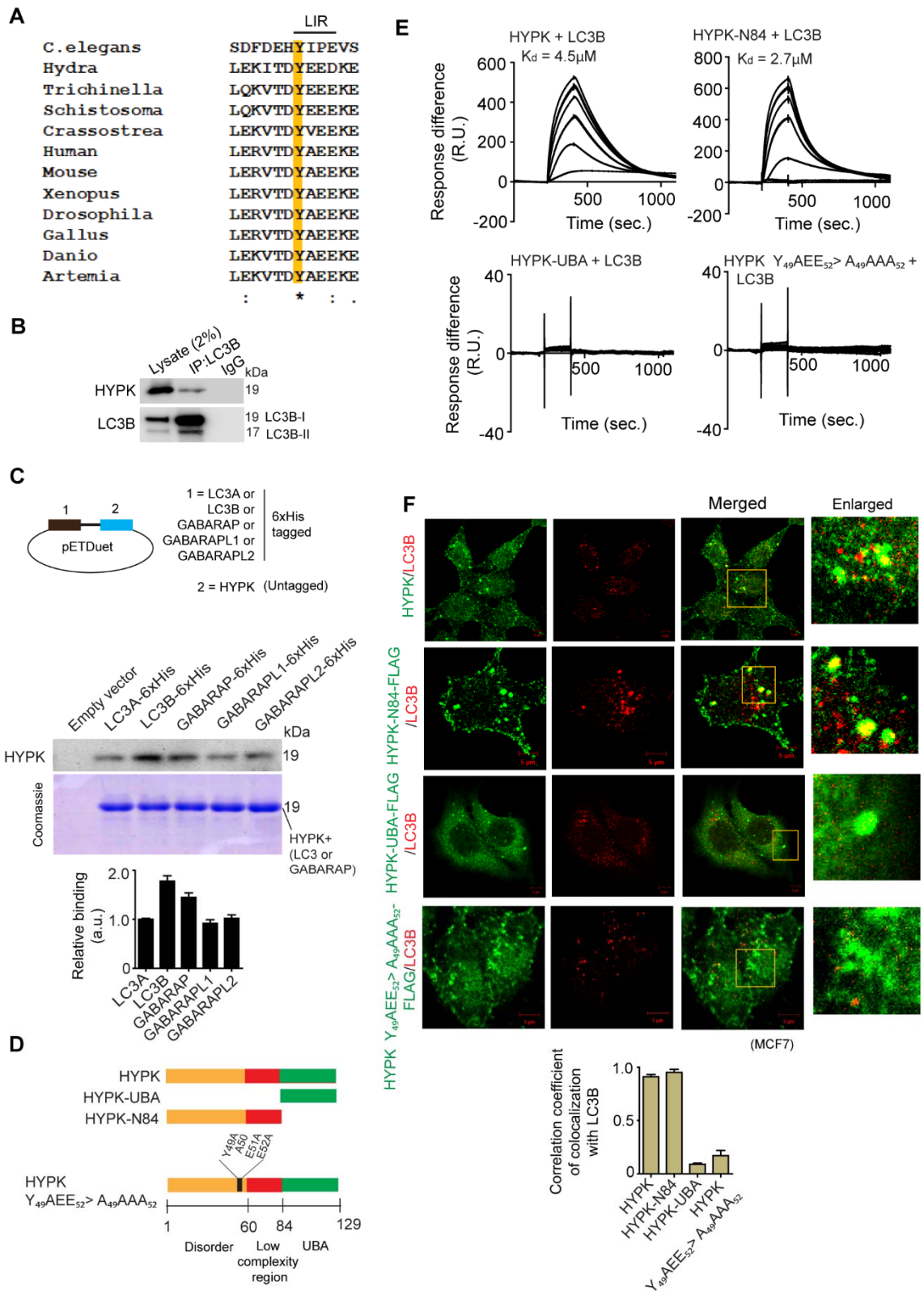

Figure 5. HYPK is a LC3 binding protein. (A) Multiple sequence alignment of the putative LC3 interacting region sequences of HYPK of different organisms. (B) Representative immunoblots of HYPK and LC3B

1123 from the non-denaturing immunocomplexes of endogenous LC3B from cell lysate of MCF7 cells. (C) Top:
1124 schematic representation of cloning of LC3A/LC3B/GABARAP/GABARAPL1/GABARAPL2 and HYPK in
1125 pETDuet-1 vector. Bottom: protein-protein interaction analysis by Ni-NTA binding of recombinant
1126 6xhistidin-tagged LC3A/LC3B/GABARAP/ GABARAPL1/GABARAPL2 and untagged HYPK coexpressed in
1127 BL21DE3 strain of *Escherichia coli* from pETDuet-1 vector. Immunoblot of HYPK and coomassie blue
1128 staining of interacting pairs; empty vector was used for negative control. (D) Representation of HYPK
1129 and its mutants used in this part of study. HYPK-UBA was the C-terminal 45 residue region, HYPK-N84
1130 was the N-terminal 84 amino acid region, the 49th, 51st and 52nd residues of HYPK were mutated to
1131 alanine in HYPK $Y_{49}AEE_{52}$>$A_{49}AAA_{52}$. (E) Quantitative analysis of binding interaction and affinities
1132 between recombinant HYPK/HYPK-UBA/HYPK-N84/HYPK $Y_{49}AEE_{52}$>$A_{49}AAA_{52}$ and LC3B determined by
1133 surface plasmon resonance assays. Dissociation constants [K_d value] were calculated by using 1:1
1134 Langmuir model of binding. (F) MCF7 cells were transfected with HYPK/HYPK-UBA/HYPK-N84/HYPK
1135 $Y_{49}AEE_{52}$>$A_{49}AAA_{52}$. Confocal immunofluorescence microscopy images of HYPK, FLAG-tagged HYPK-UBA,
1136 FLAG-tagged HYPK-N84 and FLAG-tagged HYPK $Y_{49}AEE_{52}$>$A_{49}AAA_{52}$ and LC3B. Quantitative estimation of
1137 colocalization coefficient between proteins; ~ 200 cells analysed in each sample.

1138 [α-tubulin is loading control in immunoblots. Scale bars in confocal microscopy images represent 5µm.
1139 All the presented microscopy and immunoblot data are representative of at least three independent
1140 experiments.]

1141

1142

1143

1144

1145

1146

1147

1148

1149

1150

1151

1152

1153

1154

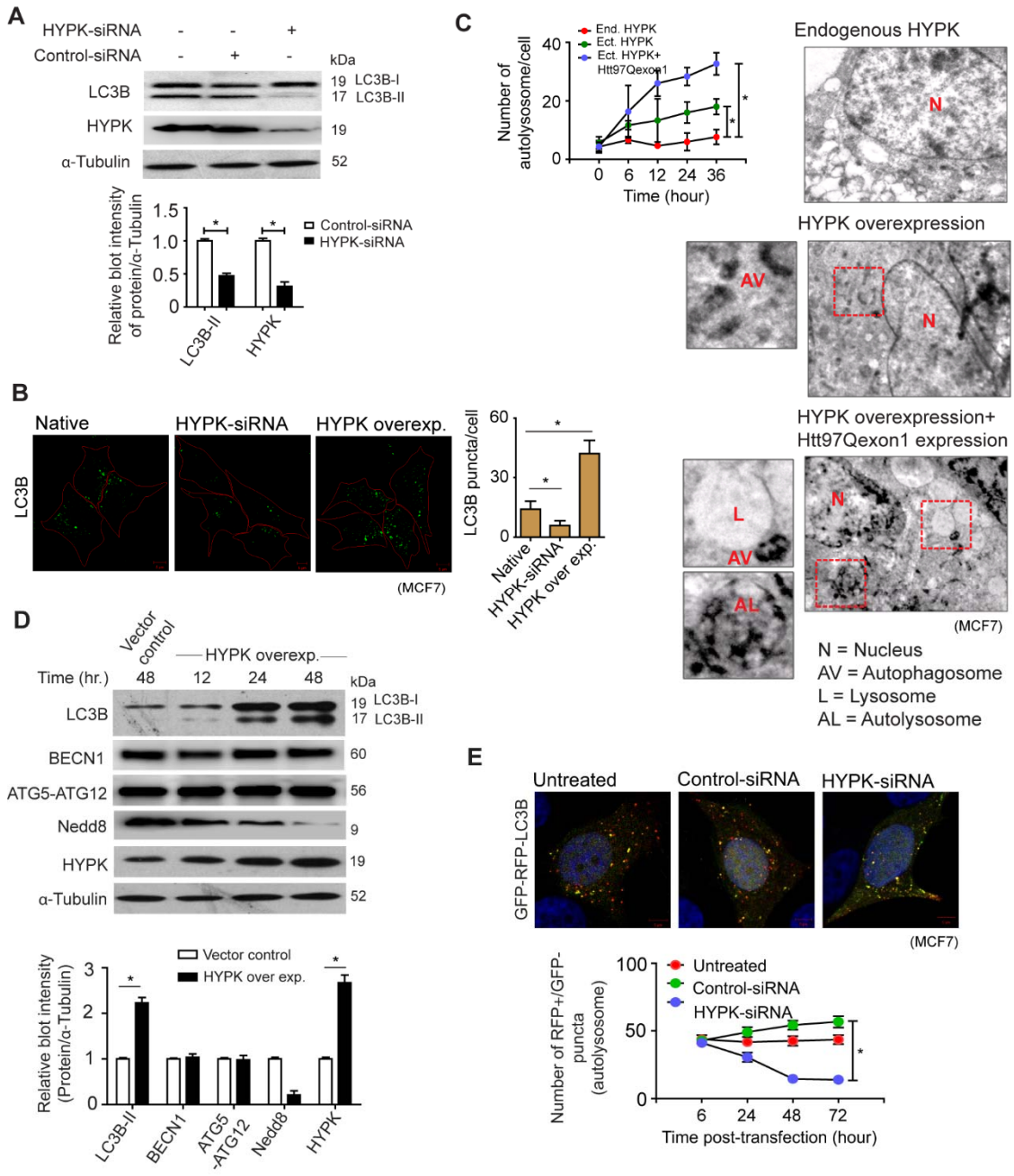

Figure 6. HYPK regulates initiation and flux of basal autophagy. (A) MCF7 cells were untransfected or transfected with control or HYPK siRNAs. Representative immunoblot of LC3B and HYPK from cell lysate. Densitometric quantification of LC3B-II and HYPK bands relative to α-tubulin of blots [* P<0.05]. (B) MCF7 cells were untransfected or transfected with HYPK siRNA or HYPK overexpressing clone. Confocal immunofluorescence microscopy images of LC3B puncta representing potential autophagosomes in cells. Quantification [mean ± SD] of number of LC3B puncta in cells; ~ 200 cells analysed in each sample [* P<0.05]. (C) Representative transmission electron micrographs of ultra-structures in MCF7 cells. Cells in the -upper panel: untreated, middle panel: transfected with HYPK overexpressing clone, lower panel: transfected with HYPK and htt97Qexon1 overexpressing clones. Quantitative [mean ± SD] estimation of

1165 autolysosomes in the above-mentioned cells for a timescale as mentioned in the figure, ~ 150 cells
1166 analysed in each sample [* P<0.05]. (D) MCF7 cells were transfected with empty vector or HYPK
1167 overexpressing clones. Representative immunoblot of LC3B, BECN1, ATG5, NEdd8 and HYPK of time-
1168 chase experiments from cell lysate. Densitometric quantification of bands of above-mentioned proteins
1169 relative to α-tubulin of blots [* P<0.05]. (E) Stable RFP-GFP-LC3B expressing MCF7 cells were
1170 untransfected or transfected with control or HYPK siRNAs. Confocal fluorescence microscopy images of
1171 GFP+/RFP+ LC3B autophagosomes and GFP-/RFP+ LC3B autolysosomes. Quantitative count [mean ± SD]
1172 of GFP-/RFP+ LC3B autolysosomes; ~ 100 cells analysed in each sample [* P<0.05].

1173 [α-tubulin is loading control in immunoblots. Scale bars in confocal microscopy images represent 5µm.
1174 All the presented microscopy and immunoblot data are representative of at least three independent
1175 experiments.]

1176

1177

1178

1179

1180

1181

1182

1183

1184

1185

1186

1187

1188

1189

1190

1191

1192

1193

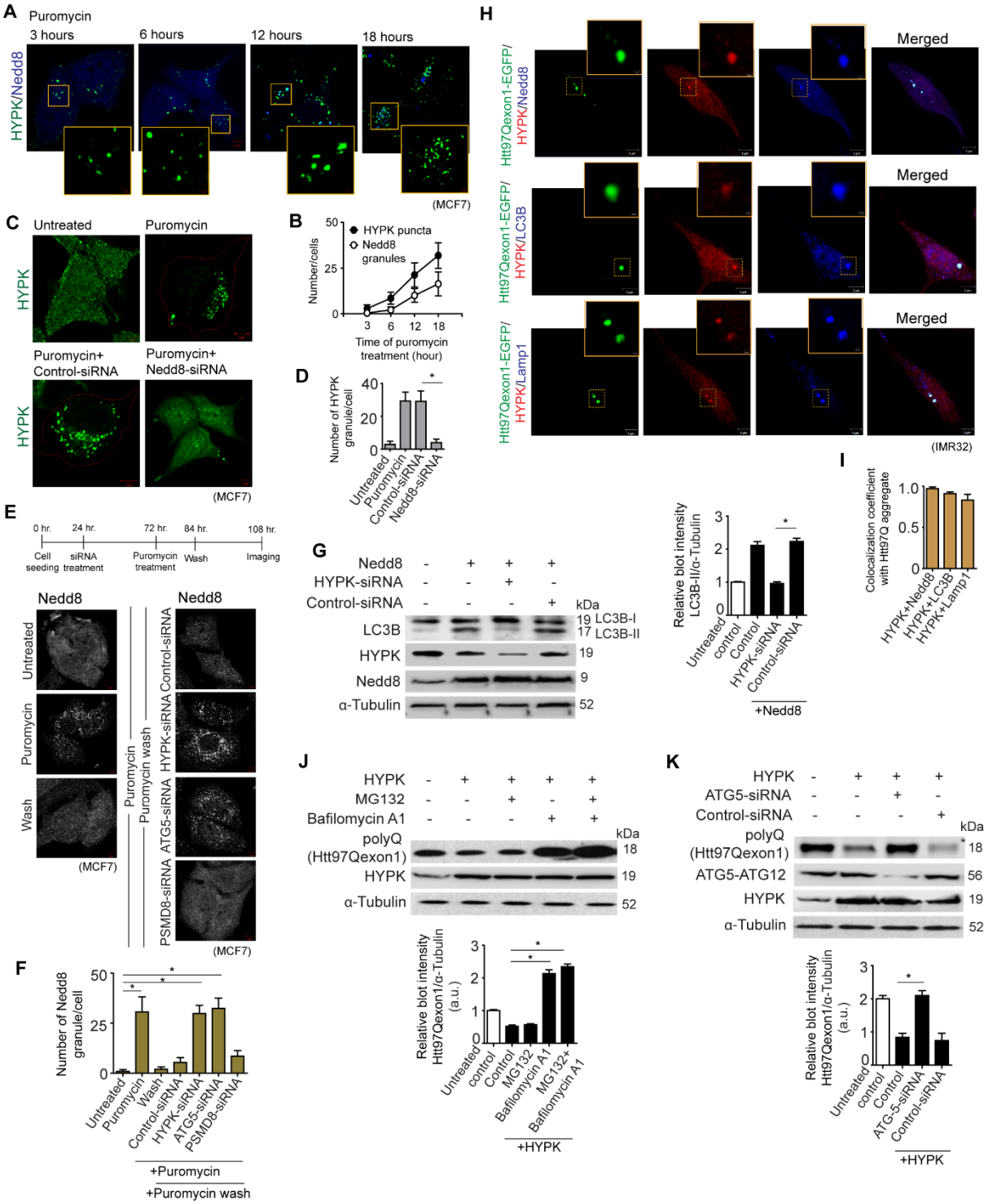

Figure 7. HYPK clears toxic aggregates of htt97Qexon1 by polyneddylation-dependent aggrephagy. (A) MCF7 cells were treated with puromycin [15µg/ml] for 0-18 hours. Confocal immunofluorescence microscopy images of HYPK and Nedd8. Inset shows enlarged region of HYPK and Nedd8 colocalized granules marked with yellow rectangles. (B) Quantification of HYPK and Nedd8 positive granules in the MCF7 cells with conditions as described in (a), ~ 100 cells analysed in each sample. (C) MCF7 cells were

1200 untreated or treated with [15µg/ml] puromycin for 24 hours. Puromycin treatment was done in
1201 untransfected or control or Nedd8 siRNA-transfected cells. Confocal immunofluorescence microscopy
1202 images of HYPK. (D) Quantification [mean ± SD] of HYPK granules in MCF7 cells with conditions as
1203 described in (c), ~ 100 cells analysed in each sample [* P<0.05]. (E and F) MCF7 cells were untransfected
1204 or transfected with control or HYPK or ATG5 or PSMD8 siRNA. Cells were treated with [15µg/ml]
1205 puromycin, followed by washout of puromycin as described in the timeline of the experiment. E:
1206 confocal immunofluorescence microscopy images of Nedd8. F: quantification of Nedd8 granules in cells
1207 with conditions as described in (e), ~ 100 cells analysed in each sample [* P<0.05]. (G) Control or HYPK
1208 siRNA was transfected in Nedd8 overexpressing MCF7 cells. Left: representative immunoblots of LC3B,
1209 HYPK and Nedd8 from the lysates of untransfected or transfected cells. Right: Densitometric
1210 quantification of LC3B-II bands relative to α-tubulin of blots [* P<0.05]. (H) Confocal
1211 immunofluorescence microscopy images of HYPK, Nedd8, LC3B and Lamp1 in stable htt97Qexon1-GFP
1212 expressing IMR-32 cells. (I) Coefficient of colocalization of HYPK, Nedd8, LC3B and Lamp1 with
1213 htt97Qexon1-GFP, ~ 100 cells analysed in each sample. (J) 5µM MG132 or 1µM bafilomycin-A1 was
1214 separately given for 24 hours to stable htt97Qexon1 expressing IMR-32 cells that were untransfected or
1215 transfected with HYPK overexpressing clone. Representative immunoblots of htt97Qexon1 and HYPK.
1216 Densitometric quantification of htt97Qexon1 bands relative to α-tubulin of blots [* P<0.05]. (K) Control
1217 or ATG5 siRNA were transfected in stable htt97Qexon1 expressing IMR-32 cells that also had HYPK
1218 overexpressing clone. Representative immunoblot of htt97Qexon1, ATG5-ATG12 and HYPK.
1219 Densitometric quantification of htt97Qexon1 bands relative to α-tubulin of blots [* P<0.05].

1220 [α-tubulin is loading control in immunoblots. Scale bars in confocal microscopy images represent 5µm.
1221 All the presented microscopy and immunoblot data are representative of at least three independent
1222 experiments.]

1223

1224

1225

1226

1227

1228

1229

1230

1231

1232

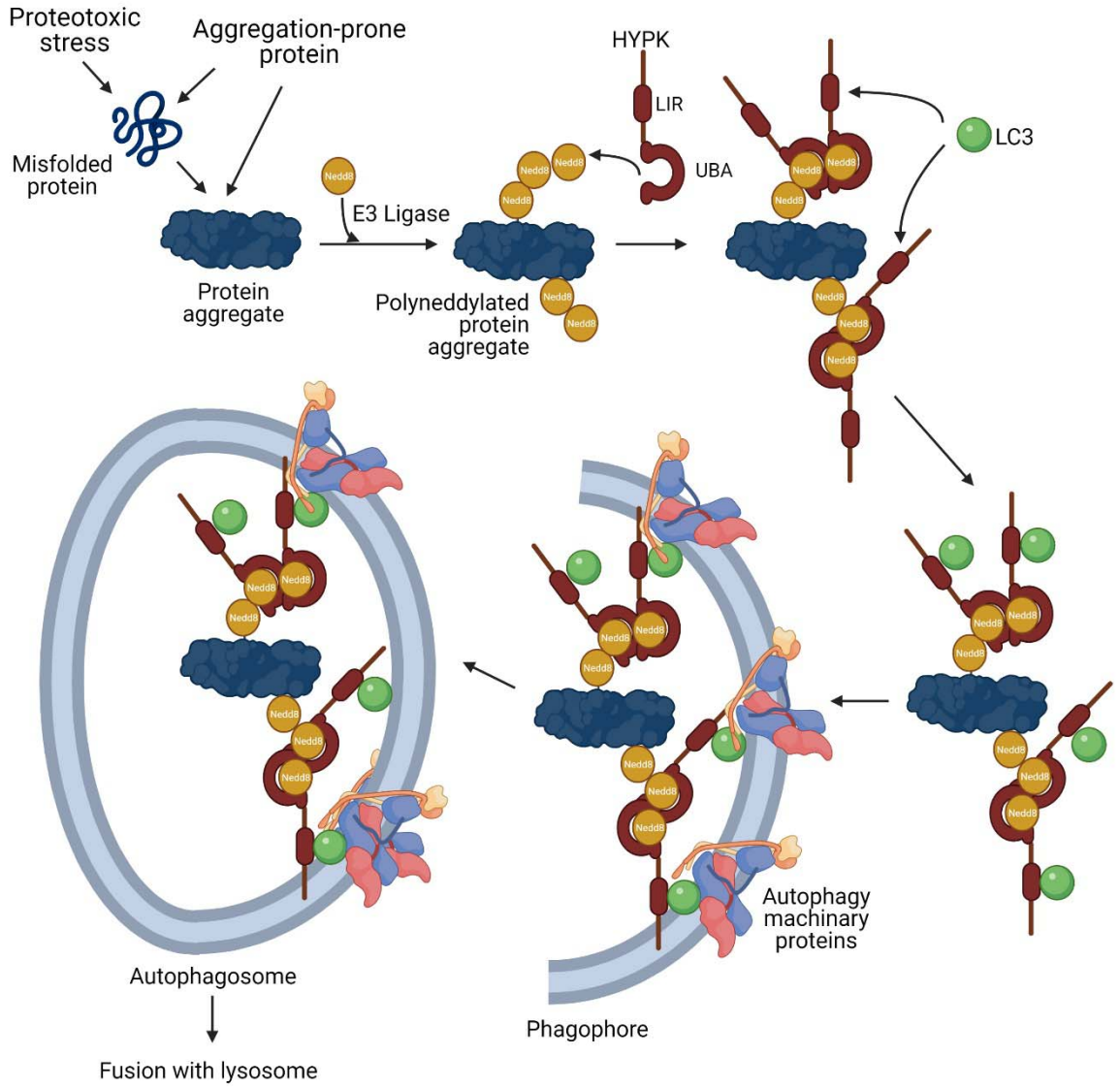

Figure 8. Model of neddylation-dependent aggrephagy and the role of HYPK in this process. In conditions of intrinsic or extrinsic proteotoxic stress, intracellular protein aggregates are progressively neddylated. HYPK binds to the Nedd8 of the polyneddylated protein aggregates by using its C-terminal UBA domain, followed by recruitment of LC3 to the site by HYPK's LIR. This promotes autophagosomal enclosing of the neddylated protein aggregates for their subsequent degradation upon delivery to lysosome.

SUPPORTING FIGURES AND LEGENDS

```
Ubiquitin      MQIFVKTLTGKTITLEVEPSDTIENVKAKIQDKEGIPPDQQRLIFAGKQLEDGRTLSDYNIQKESTLHLVLRLRGG----- 76
Nedd8          MLIKVKTLTGKEIEIDIEPTDKVERIKERVEEKEGIPPQQQRLIYSGKQMNDEKTAADYKILGGSVLHLVLALRGGGGLRQ 81
               * * ******* * :::**:*.:*.:* ::::******:*****::***::* :* :**:*   *.***** ****

Ubiquitin      ---------------------MQIFVKTLTGKTITLEVEPSDTIENVKAKIQDKEGIPPDQQRLIFAGKQLEDGRTLSDYNIQKESTLHLVLRLRGG----    76
SUMO1          MSDQEAKPSTEDLGDKKEGEYIKLKVIGQDSSEIHFKVKMTTHLKKLKESYCQRQGVPMNSLRFLFEGQRIADNHTPKELGMEEEDVIEVYQEQTGGHSTV    101
                                     ::: *    .. * ::*: :  ::::* .  :::*:* :. *::* *::: *.:* .: .:::*..:.:  .  **

Ubiquitin      ------------------------------------------------------------------------------------MQIFVK--TLTGKTITLEVEPSDTIENVKAKIQ
FAT10          MAPNASCLCVHVRSEEWDLMTFDANPYDSVKKIKEHVRSKTKVPVQDQVLLLGSKILKPRRSLSSYGIDKEKTIHLTLKVVKPSDEELPLFLVESGDEAKRHLLQVRRSSSVAQVKAMIE
                                                                                                                  : :*:      .*   *:*. *.:: :*** *:
               Ubiquitin      DKEGIPPDQQRLIFAGKQLEDGRTLSDYNIQKESTLHLVLRLRGG   76
               FAT10          TKTGIIPETQIVTCNGKRLEDGKMMADYGIRKGNLLFLACYCIGG   165
                               * ** *: * :   **:****: ::**.*:* . *.*.    **

Ubiquitin      --------------MQIFVKTLTGKTITLE--VEPSDTIENVKAKIQDKEGIPPDQQRLIFAGKQLEDGR------------TLSDYNIQKESTLHLVLRLRGG    76
URM1           MAAPLSVEVEFGGGAELLFDGIKKHRVTLPGQEEPWD-IRNLL--IWIKKNLLKERPELFIQGDSVRPGILVLINDADWELLGELDYQLQDQDSVLFISTLHGG    101
                              ::: .. :. : :**    ** * *.*:   *  *:.:  :: .*:: *..:. *               **::*.:.:: ::  *:**

Ubiquitin      MQIFVKTLTGKTITLEVEPSDTIENVKAKIQDKEGIPPDQQRLIFAGKQLEDGRTLSDYNIQKESTLHLVLRLRGG-------------------------------------------
S27A           MQIFVKTLTGKTITLEVEPSDTIENVKAKIQDKEGIPPDQQRLIFAGKQLEDGRTLSDYNIQKESTLHLVLRLRGGAKKRKKKSYTTPKKNKHKRKKVKLAVLKYYKVDENGKISRLRRE
               ***********************************************************************

               Ubiquitin      ------------------------------------    76
               S27A           CPSDECGAGVFMASHFDRHYCGKCCLTYCFNKPEDK    156
```

Supporting figure 1. Sequence alignment of ubiquitin with different ubiquitin-like proteins.

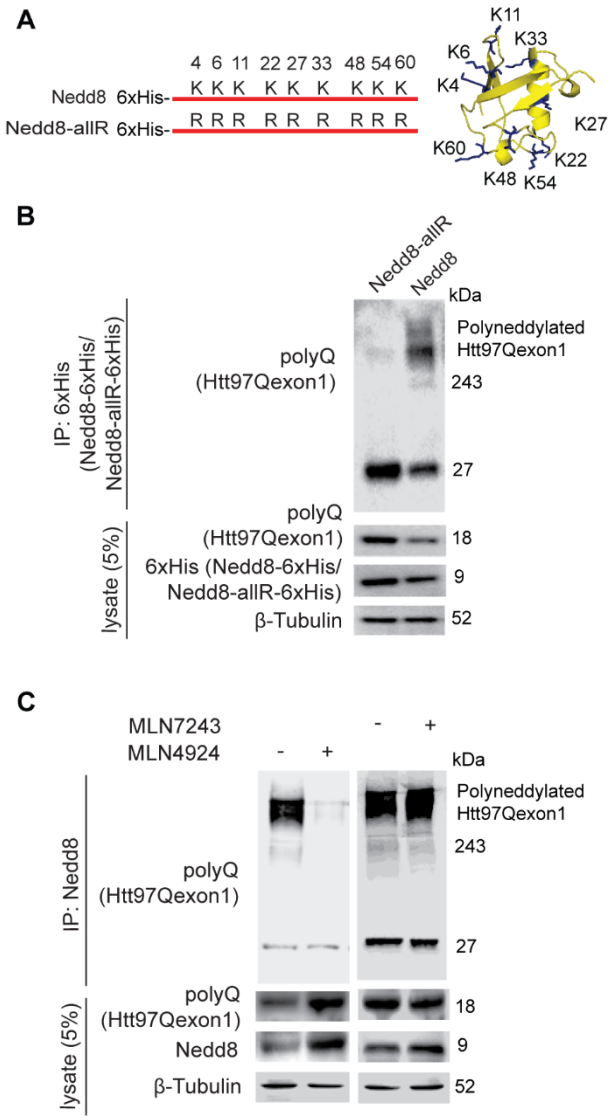

Supporting figure 2. Htt97Qexon1 undergoes homogeneous polyneddylation. (A) Left: schematic representation of wild type and mutant Nedd8 constructs. In the Nedd8-allR mutant, all the lysine residues were arginine. Positions of lysine residues in the wild-type human Nedd8 are indicated. Right: crystal structure of Nedd8 [84] with lysine residues indicated with stick structure. (B) Representative Immunoblots of htt97Qexon1, 6xHis-tagged Nedd8 and 6xHis-tagged Nedd8-allR of immunocomplexes of 6xHis-Nedd8 and 6xHis-Nedd8-allR from lysate of stable htt97Qexon1 expressing IMR-32 cells. (C) Stable htt97Qexon1 expressing IMR-32 cells were treated with 1µM MLN4924 or 1µM MLN7243 for 24 hours. Representative Immunoblots of htt97Qexon1 and Nedd8 of immunocomplexes of Nedd8 from lysate of the above-mentioned cells.

[β-tubulin is loading control in immunoblots. Immunoblot data are representative of at least three independent experiments.]

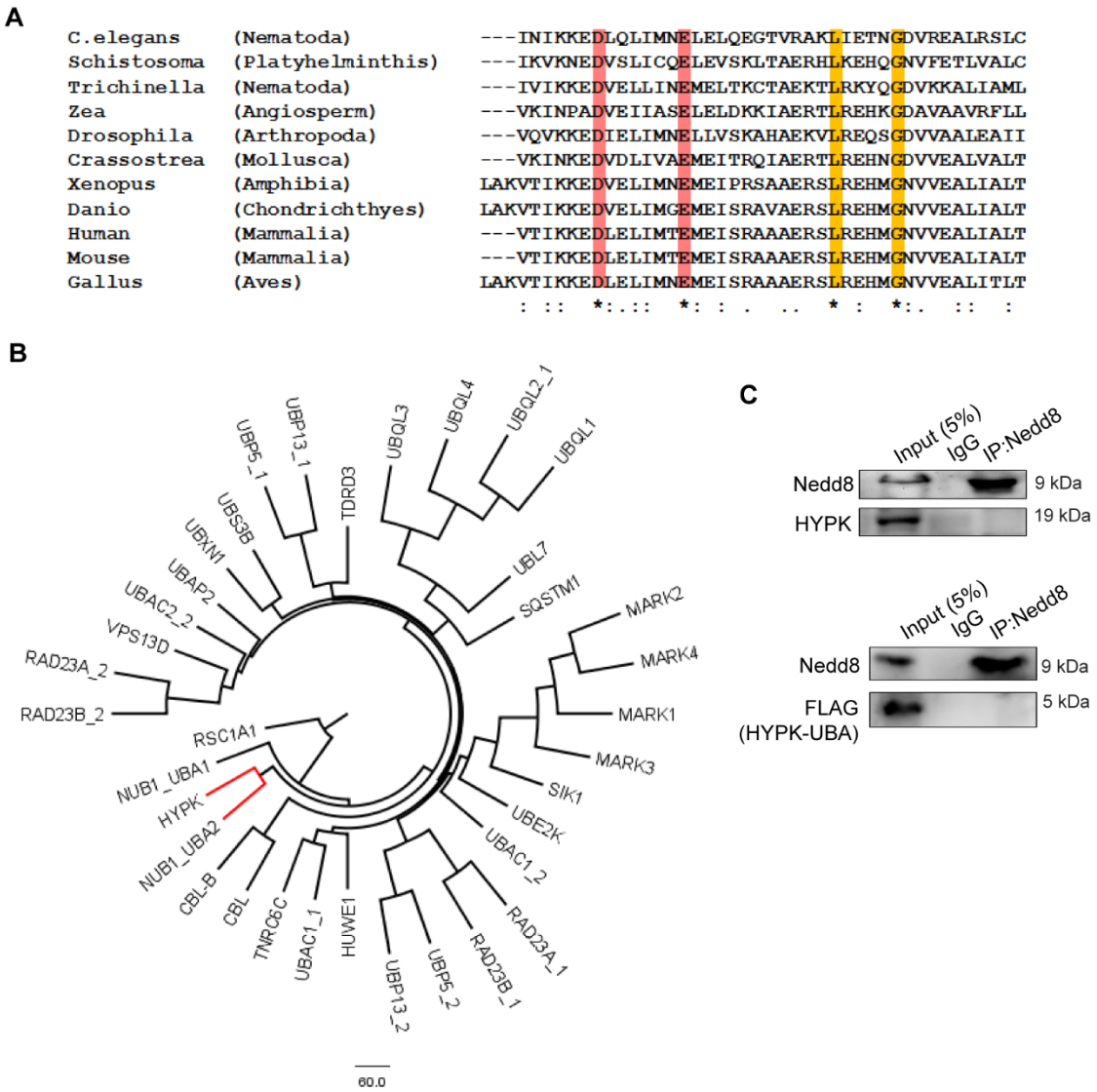

Supporting figure 3. The conserved UBA domain of HYPK noncovalently binds to Nedd8. (A) Multiple sequence alignment of the UBA domains of HYPK proteins of different organisms. Conserved charged and hydrophobic amino acids are highlighted with red and yellow colour respectively. (B) Cladogram representing the clustered UBA domains of different human proteins. Scale indicates phylogenetic distance. (C) Representative immunoblots of Nedd8, HYPK and FLAG-tagged HYPK-UBA [ectopically expressed] of denaturing immunoprecipitation of Nedd8 from lysate of MCF7 cells.

[Immunoblot data are representative of at least three independent experiments.]

1287 **Supporting table 1. HYPK transcript expression level in different neurodegenerative and brain**
1288 **diseases.**
1289

Disease / disease model	GEO number	HYPK expression altered	Remarks	Reference
Parkinson's disease: substantia nigra	GDS2821	No	-	94
X-linked recessive dystonia-parkinsonism	GDS1912	No	-	Unpublished
Alzheimer's disease: neurofibrillary tangles	GDS2795	No	-	95
HdhQ111 knock-in model of Huntington's disease: striatum	GDS4534	No	-	96
Amyotrophic lateral sclerosis model	GDS3408	No	-	97
Frontotemporal lobar degeneration with ubiquitinated inclusions and progranulin mutations: various brain regions - TDP-43	GDS3459	Yes	Downregulated	98
Amyloid Precursor Protein APP family members: adult prefrontal cortex	GDS4414	Yes	Upregulated	99
Spinocerebellar ataxia type 7 knock-in model: cerebellum - Spinocerebellar ataxia	GDS3545	No	-	100
Spinocerebellar ataxia type 1 knock-in model: cerebellum	GDS3544	No	-	100
Multiple sclerosis: brain lesions	GDS4218	Yes	Downregulated	101
Down syndrome: brain	GDS2941	Yes	Downregulated	102
Cerebellar cortex in schizophrenia	GDS1917	NO	-	
Measles virus brain infection model: right cerebral hemisphere	GDS4553	Yes	Upregulated	103
Simian immunodeficiency virus encephalitis model of HIV-associated dementia: hippocampus - Dementia	GDS4214	No	-	104
Progressive diabetic neuropathy: sural nerve	GDS4012	No	-	105

1290